

# The Spin-MInt Algorithm: an Accurate and Symplectic Propagator for the Spin-Mapping Representation of Nonadiabatic Dynamics

Lauren E. Cook,<sup>1</sup> James R. Rampton,<sup>1</sup> and Timothy J. H. Hele<sup>1, a)</sup>

*Department of Chemistry, University College London, Christopher Ingold Building,  
London WC1H 0AJ, United Kingdom*

(Dated: 2 December 2025)

Mapping methods, including the Meyer–Miller–Stock–Thoss (MMST) mapping and spin-mapping, are commonly utilised to simulate nonadiabatic dynamics by propagating classical mapping variable trajectories. Recent work confirmed the Momentum Integral (MInt) algorithm is the only known *symplectic* algorithm for the MMST Hamiltonian. To our knowledge, no symplectic algorithm has been published for the spin-mapping representation without converting to MMST variables and utilising the MInt algorithm. Here, we present the Spin-MInt algorithm which directly propagates the spin-mapping variables. First, we consider a two-level system which maps onto a spin-vector on a Bloch sphere and determine that the Spin-MInt is a *symplectic, symmetrical, second-order, time-reversible, angle invariant and geometric structure preserving* algorithm. Despite spin-variables resulting in a non-invertible structure matrix, we rigorously prove the Spin-MInt is symplectic using a canonical variable transformation. Computationally, we find that the Spin-MInt and MInt algorithms are symplectic, satisfy Liouville’s theorem, provide second-order energy conservation and are more accurate than a previously-published angle-based algorithm. The Spin-MInt is significantly faster than the MInt algorithm for two electronic states. Secondly, we extend this methodology to more than two electronic states and present accurate population results for a three-state morse potential. We believe this to be the *first known symplectic* algorithm for propagating the nonadiabatic spin-mapping Hamiltonian and one of the first rigorously symplectic algorithms in the case of non-trivial coupling between canonical and spin systems. These results should guide and improve future simulations.

---

<sup>a)</sup>Electronic mail: t.hele@ucl.ac.uk

# I. INTRODUCTION

Nonadiabatic dynamics governs many interesting phenomena involving light and energy transfer. Simulation is particularly challenging to implement due to the coupled nuclear and electronic degrees of freedom (DoF). Full quantum methods, such as Multi-Configurational Time-Dependent Hartree Fock (MCTDH) and wavepacket methods,<sup>1–5</sup> are extremely accurate but limited to smaller systems by the large computational expense associated. For single surface (adiabatic) systems, many classical-scaling methods have been introduced including ring-polymer molecular dynamics (RPMD), the associated centroid molecular dynamics (CMD) and thermostatted (T)-RPMD, and the Linearised Semiclassical Initial-Value Representations (LSC-IVR).<sup>6–26</sup> Several extensions for nonadiabatic dynamics are available such as mean-field RPMD, nonadiabatic (N)-RPMD and mapping variable (MV)-RPMD for RPMD,<sup>27–29</sup> and Mixed Quantum Classical (MCQ)-IVR for IVR methods.<sup>30–35</sup> Additionally, several mixed quantum-classical methods exist including Ehrenfest methods, surface hopping and mapping methods.<sup>12,36–48</sup>

Here, we focus on trajectory-based mapping methods which map the discrete quantum system onto continuous variables which can be propagated classically. One well-established method is the Meyer-Miller-Stock-Thoss (MMST) mapping which obtains electronic positions and momenta and evolves under the MMST Hamiltonian using Hamilton’s equations of motion (EOM).<sup>12,42</sup> Alternatively, spin-mapping obtains a spin-vector on the surface of a Bloch sphere (in the two-level case) which follows Heisenberg’s EOM.<sup>44,49,50</sup> This is an advantageous representation as it removes two redundant DoF compared to the MMST representation.<sup>44,49</sup> The two representations are related, where elements of the spin-vector can be calculated from MMST variables and the Hamiltonians are equivalent under the addition of a zero-point energy (ZPE) parameter to the MMST Hamiltonian.<sup>44,49,51</sup> A ZPE fitting parameter was first introduced by Stock and Müller to mitigate ZPE leakage and many possibilities were tested.<sup>52,53</sup> However, spin-mapping derives this as a function of the number of states and leads to a parameter that is close to what was previously found to be optimal.<sup>44</sup>

Historically, spin-mapping was limited to two electronic states.<sup>44,54</sup> However, spin-coherent states and the  $SU(N)$  Lie group have been harnessed to generalise to more states and we use this approach to extend this work.<sup>49,51,55</sup> While many of the nonadiabatic ring-polymer methods utilise the MMST mapping, a spin-mapping (SM)-NRPMD has been proposed,<sup>54,55</sup> which alongside the flurry of spin-mapping methods including a partially linearized approach,<sup>56–58</sup> an ellipsoidal

method,<sup>59</sup> generalisation to multiple states,<sup>49,51,55</sup> and the Mapping Approach to Surface Hopping (MASH), highlights the interest in spin-mapping approaches.<sup>45,60–64</sup> As far as we are aware, none of the mapping methods developed thus far reproduce Rabi oscillations, scale classically with system size, conserve the quantum Boltzmann distribution, have a clear derivation from exact quantum dynamics and produce accurate dynamics.<sup>65</sup> Recent work showed that such a method is unlikely to be obtained through use of MMST variables and the related electronic state descriptors but an alternative metric, such as a spin-mapping metric, may achieve this in future.<sup>65</sup>

To investigate dynamical properties of nonadiabatic systems, mapping methods are often utilised to approximate correlation functions of the form,

$$C_{AB} = \frac{1}{Z} \text{Tr}[e^{-\beta \hat{H}} \hat{A}(0) \hat{B}(t)], \quad (1)$$

where  $e^{-\beta \hat{H}}$  is the quantum Boltzmann distribution at inverse temperature,  $\beta = 1/k_B T$ ,  $\hat{A}$  and  $\hat{B}$  are operators and  $Z$  is the partition function given by,

$$Z = \text{Tr}[e^{-\beta \hat{H}}]. \quad (2)$$

To approximate these, many molecular dynamics trajectories are required to ensure that enough phase-space is sampled. Therefore, we need accurate propagation algorithms.<sup>66</sup>

For Hamiltonian systems, algorithms can be *symplectic* which arises from exact Hamiltonian or sub-Hamiltonian integration and results in no/little energy drift over time when propagating the dynamics.<sup>67</sup> This is also advantageous for methods that have a phase-factor as a symplectic integrator aids convergence.<sup>13,68,69</sup> Although many algorithms have been developed for the MMST Hamiltonian,<sup>26,68,70,71</sup> a recent study has shown that the MInt algorithm is the only rigorously symplectic integrator.<sup>66,68</sup> As far as we are aware, no such algorithm has been proposed for the spin-mapping representation.<sup>44</sup> While an angle-based algorithm has been utilised for the spin-mapping Hamiltonian, it is known to have instabilities and it was subsequently suggested that to obtain symplectic propagation, one should transform into MMST variables and propagate with the MInt algorithm before transforming back.<sup>49,51,54</sup> Therefore, we believe it would be advantageous to be able to propagate the spin-variables directly for the spin-mapping Hamiltonian to reduce both the computational cost and the opportunity for errors to arise. Other algorithms have been suggested for general spin-systems,<sup>72–78</sup> but many assume a separable Hamiltonian, use a Split-Liouvillian approximation (which we later show results in a loss of symplecticity for the spin-mapping Hamiltonian) or are not applicable to a system with a non-trivial coupling between the nuclear and electronic DoF. Hence, we do not consider them further in this work.

In this article, we present a spin-mapping approach to the MInt algorithm (the Spin-MInt algorithm) which we believe to be the first symplectic algorithm for the spin-mapping Hamiltonian, following a similar flowmap to the MInt algorithm and inheriting many of its properties. The structure of this article is as follows. In section II, we present background theory, including the MInt algorithm and spin-mapping. In section III, we present the methodology of the Spin-MInt algorithm (generalised to  $N$  states in Appendix E) and its properties. Algebraically, we determine that the Spin-MInt is symplectic via a canonical variable transformation.<sup>51</sup> In section IV, we present computational results. For a two-level system, we compare a single trajectory using the Spin-MInt, MInt and an angle-based algorithm.<sup>51,54,66,68</sup> The Spin-MInt and MInt algorithms produce identical evolution and are more accurate than the angle-based algorithm. For an ensemble of trajectories, we compare position and electronic population auto-correlation functions, satisfaction of Liouville's theorem, symplecticity and energy conservation for the Spin-MInt and MInt algorithms. Additionally, for a three-state Morse potential, we present population dynamics in agreement with the exact result. We find that for the two-level system, the Spin-MInt is significantly faster than the MInt algorithm. We conclude in section V.

## II. BACKGROUND THEORY

Here, we present the background theory of the MMST mapping, the MInt algorithm and spin-mapping. As spin-mapping was first introduced for a two state system,<sup>44</sup> resulting in a three dimensional spin-vector, we present this section with one nuclear and two electronic DoF. This also allows easy computational comparison between algorithms on the simplest system.<sup>66</sup>

### A. MMST Representation

#### 1. MMST Hamiltonian

The MMST Hamiltonian is

$$H_{\text{MMST}} = \frac{P^2}{2m} + V_0(R) + \frac{1}{2} \{ \mathbf{p}^T \mathbf{V}(R) \mathbf{p} + \mathbf{q}^T \mathbf{V}(R) \mathbf{q} - \gamma \text{Tr}[\mathbf{V}(R)] \}, \quad (3)$$

where  $R$  and  $P$  are the nuclear position and momenta and the mapping variables,  $\mathbf{q}$  and  $\mathbf{p}$ , are the electronic position and momenta. The ZPE parameter,  $\gamma$ , introduced by Stock and Müller to reduce ZPE-leakage, is unity in the standard MMST mapping.<sup>52</sup> ZPE-leakage occurs when energy

unphysically flows between states.<sup>66</sup> The diabatic potentials,  $V_0(R)$  and  $\mathbf{V}(R)$ , are dependent on nuclear position and are the state-independent and state-dependent potentials respectively. For a two-level system,  $\mathbf{V}(R)$  typically has the following form,

$$\mathbf{V}(R) = \begin{bmatrix} V_1(R) & \Delta^*(R) \\ \Delta(R) & V_2(R) \end{bmatrix}, \quad (4)$$

where  $\Delta$  is the coupling between electronic states,  $*$  represents the complex conjugate and  $V_{1/2}$  are the state energies.

## 2. MInt Algorithm

The MInt algorithm is the only known symplectic algorithm for propagation of the MMST Hamiltonian.<sup>66,68</sup> The Hamiltonian is split into two parts such that,

$$H_{1,\text{MMST}} = \frac{P^2}{2m}, \quad (5a)$$

$$H_{2,\text{MMST}} = V_0(R) + \frac{1}{2} \{ \mathbf{p}^T \mathbf{V}(R) \mathbf{p} + \mathbf{q}^T \mathbf{V}(R) \mathbf{q} - \gamma \text{Tr}[\mathbf{V}(R)] \}, \quad (5b)$$

and the MInt algorithm integrates both sub-Hamiltonians exactly. Here, we derive the MInt algorithm with the ZPE parameter such that it can be directly compared with the Spin-MInt algorithm. One may note that if the diabatic potential matrix is traceless,  $\mathbf{V}(R)$ , which is common in spin-mapping approaches,<sup>44</sup> this term is zero. The flow map for the algorithm is as follows,<sup>66,68</sup>

$$\Psi_{H,\Delta t}^{\text{MInt}} := \Phi_{H_{1,\text{MMST}},\Delta t/2} \circ \Phi_{H_{2,\text{MMST}},\Delta t} \circ \Phi_{H_{1,\text{MMST}},\Delta t/2}, \quad (6)$$

where the overall evolution for a timestep,  $\Delta t$ , is performed by sandwiching the evolution of  $H_{2,\text{MMST}}$  with two half timestep evolutions of  $H_{1,\text{MMST}}$ . In this notation  $\Phi$  represents exact sub-evolution and  $\Psi$  is approximate evolution.<sup>66</sup> Evolution can be performed with the two sub-Hamiltonians swapped at an increased computational cost.<sup>66,68</sup>

The propagation equations are based on Hamilton's EOM where,<sup>12,43,66</sup>

$$\dot{R} = \frac{\partial H}{\partial P}, \quad \dot{P} = -\frac{\partial H}{\partial R}, \quad (7a)$$

$$\dot{\mathbf{q}} = \frac{\partial H}{\partial \mathbf{p}}, \quad \dot{\mathbf{p}} = -\frac{\partial H}{\partial \mathbf{q}}, \quad (7b)$$

which can be integrated exactly for each sub-Hamiltonian.

For  $H_{1,\text{MMST}}$ , the only propagated variable is the nuclear position where,

$$R(t + \Delta t/2) = R(t) + \frac{P}{2m}\Delta t, \quad (8)$$

and all other variables are unchanged.<sup>66,68</sup>

For  $H_{2,\text{MMST}}$ , the nuclear position is unchanged and all other variables are propagated using,

$$\dot{P} = -V'_0(R) - \frac{1}{2} \{ (\mathbf{q} - i\mathbf{p})^T \mathbf{V}'(R) (\mathbf{q} + i\mathbf{p}) - \gamma \text{Tr}[\mathbf{V}'(R)] \}, \quad (9a)$$

$$\dot{\mathbf{q}} = \mathbf{V}\mathbf{p} \quad , \quad \dot{\mathbf{p}} = -\mathbf{V}\mathbf{q}, \quad (9b)$$

where the prime indicates the derivative with respect to  $R$ . The MInt algorithm utilises the fact that  $\dot{\mathbf{q}}$  and  $\dot{\mathbf{p}}$  are independent of  $\dot{P}$  but  $\dot{P}$  depends on  $\dot{\mathbf{q}}$  and  $\dot{\mathbf{p}}$  such that one can solve for time-evolved  $\mathbf{q}$  and  $\mathbf{p}$  and then use these values to solve for time-evolved  $P$ .<sup>66,68</sup>

The electronic propagation in Eqn. (9b) becomes,

$$[\mathbf{q} + i\mathbf{p}](t + \Delta t) = e^{-i\mathbf{V}\Delta t}[\mathbf{q} + i\mathbf{p}](t), \quad (10)$$

as is seen for many MMST integrators,<sup>28,66,68,70,71</sup> and we use the shorthand  $[\mathbf{q} + i\mathbf{p}](t) \equiv \mathbf{q}(t) + i\mathbf{p}(t)$ . The decomposition of the diabatic potential matrix is,

$$\mathbf{V} = \mathbf{S}\mathbf{\Lambda}\mathbf{S}^T, \quad (11)$$

where  $\mathbf{S}$  is the eigenvectors and  $\mathbf{\Lambda}$  is a diagonal matrix of the eigenvalues. In Section IA of the Supplementary Material, an algebraic form of  $\mathbf{S}$  and  $\mathbf{\Lambda}$  and their derivatives for the potential matrix in Eqn. (4) where  $\Delta$  is real is presented. Hence,

$$\mathbf{q}(t + \Delta t) = \mathbf{C}\mathbf{q}(t) - \mathbf{D}\mathbf{p}(t), \quad (12a)$$

$$\mathbf{p}(t + \Delta t) = \mathbf{C}\mathbf{p}(t) + \mathbf{D}\mathbf{q}(t), \quad (12b)$$

where,

$$\mathbf{C} = \mathbf{S}\cos(\mathbf{\Lambda}\Delta t)\mathbf{S}^T \quad , \quad \mathbf{D} = -\mathbf{S}\sin(\mathbf{\Lambda}\Delta t)\mathbf{S}^T. \quad (13)$$

For the nuclear momentum propagation, Eqn. (10) is used to obtain the propagation of  $P$  in terms of  $\mathbf{q}(t)$  and  $\mathbf{p}(t)$ , such that integration results in,

$$P(\Delta t) = - \left\{ V'_0(R) - \frac{\gamma}{2} \text{Tr}[\mathbf{V}'(R)] \right\} \Delta t - \frac{1}{2} \int_0^{\Delta t} dt \left\{ [\mathbf{q} - i\mathbf{p}]^T(0) e^{i\mathbf{V}\Delta t} \mathbf{V}'(R) e^{-i\mathbf{V}\Delta t} [\mathbf{q} + i\mathbf{p}](0) \right\}, \quad (14)$$

The derivative of the potential in the adiabatic basis is defined as,  $\mathbf{G} = \mathbf{S}^T \mathbf{V}' \mathbf{S}$ , and inserting  $\mathbf{S} \mathbf{S}^T$  identities into Eqn. (14) results in,

$$P(t + \Delta t) = P(t) - \left\{ V'_0(R) - \frac{\gamma}{2} \text{Tr}[\mathbf{V}'(R)] \right\} \Delta t - \frac{1}{2} \int_0^{\Delta t} dt \left\{ [\mathbf{q} - i\mathbf{p}]^T(0) \mathbf{S} e^{i\mathbf{\Lambda}t} \mathbf{G} e^{-i\mathbf{\Lambda}t} \mathbf{S}^T [\mathbf{q} + i\mathbf{p}](0) \right\}, \quad (15)$$

where the MInt approach to the integral is,

$$I = \int_0^{\Delta t} dt \quad \mathbf{S} e^{i\mathbf{\Lambda}t} \mathbf{G} e^{-i\mathbf{\Lambda}t} \mathbf{S}^T = \mathbf{E} + i\mathbf{F}. \quad (16)$$

If we define,

$$\mathbf{\Gamma}_{nm} = \begin{cases} \mathbf{\Lambda}'_{nn} \Delta t & n = m \\ -(\mathbf{S}^T \mathbf{S}')_{nm} \sin(\lambda_{nm} \Delta t) & n \neq m, \end{cases} \quad (17a)$$

$$\mathbf{\Xi}_{nm} = \begin{cases} 0 & n = m \\ [\cos(\lambda_{nm} \Delta t) - 1] (\mathbf{S}^T \mathbf{S}')_{nm} & n \neq m, \end{cases} \quad (17b)$$

where  $\lambda_{nm} = (\mathbf{\Lambda})_{mm} - (\mathbf{\Lambda})_{nn}$ , such that,

$$\mathbf{E} := \mathbf{S}^T \mathbf{\Gamma} \mathbf{S} \quad , \quad \mathbf{F} := \mathbf{S}^T \mathbf{\Xi} \mathbf{S}, \quad (18)$$

where  $\mathbf{E}$  is symmetric and  $\mathbf{F}$  is skew-symmetric.<sup>66,68</sup> The nuclear momentum propagation is then,

$$P(t + \Delta t) = P(t) - \left\{ V'_0(R) - \frac{\gamma}{2} \text{Tr}[\mathbf{V}'(R)] \right\} \Delta t - \frac{1}{2} \left\{ \mathbf{q}^T(t) \mathbf{E} \mathbf{q}(t) + \mathbf{p}^T(t) \mathbf{E} \mathbf{p}(t) - 2\mathbf{q}^T(t) \mathbf{F} \mathbf{p}(t) \right\}. \quad (19)$$

The MInt algorithm follows the flow map in Eqn. (6), propagating  $R$  with Eqn. (8) for  $H_{1,\text{MMST}}$ ,  $\mathbf{q}$  and  $\mathbf{p}$  with Eqn. (12) and  $P$  with Eqn. (19) for  $H_{2,\text{MMST}}$ . Further algorithmic details and extension to multiple states is seen in Ref. [68], where here we have used a similar notation to Ref. [66] but included the ZPE parameter,  $\gamma$ .

## B. Symplecticity

A Hamiltonian system can be described by,<sup>66-68</sup>

$$\frac{\partial \mathbf{z}}{\partial t} = \mathbf{J} \nabla_{\mathbf{z}} \mathbf{H}(\mathbf{z}, t), \quad (20)$$

where  $\mathbf{J}$  is the structure matrix and  $\mathbf{z}$  contains the system variables which for the MMST mapping is,  $\mathbf{z}^T = [R, P, \mathbf{q}^T, \mathbf{p}^T]$ . In this case where Hamilton's EOM are utilised,

$$\mathbf{J} = \begin{bmatrix} \mathbb{O} & \mathbb{I} \\ -\mathbb{I} & \mathbb{O} \end{bmatrix}, \quad (21)$$

where  $\mathbb{O}$  and  $\mathbb{I}$  are the zero and identity matrices respectively. For canonical systems, a Hamiltonian integrator is symplectic if it fulfils the following condition,<sup>66–68</sup>

$$\mathbf{M}^T \mathbf{J}^{-1} \mathbf{M} = \mathbf{J}^{-1}, \quad (22)$$

where  $\mathbf{M}$  is the monodromy matrix defined as,

$$\mathbf{M} \equiv \frac{\partial \mathbf{z}_t}{\partial \mathbf{z}_0} \quad \text{where} \quad \mathbf{M}_{\mathbf{XY}} = \frac{\partial \mathbf{X}(t)}{\partial \mathbf{Y}(0)}. \quad (23)$$

which is a matrix of differentials expressing how the time-evolved phase-space variables depend on the initial phase-space variables<sup>79</sup> This can be computed for each timestep and multiplied with the previous timestep matrices to obtain the monodromy matrix for the overall trajectory,<sup>66</sup>

$$\mathbf{M}(2\Delta t) = \mathbf{M}(\Delta t \rightarrow 2\Delta t) \mathbf{M}(0 \rightarrow \Delta t). \quad (24)$$

For a split Hamiltonian system,  $H = H_1 + H_2$ , the monodromy matrix is calculated for each timestep according to the algorithmic flow map.<sup>66,67</sup> The MInt algorithm is the only known symplectic algorithm for the MMST Hamiltonian where the criteria in Eqn. (22) is proven both algebraically and numerically.<sup>66,68</sup> We present the algebraic forms of the monodromy matrices for the MInt algorithm in Appendix A.

### C. Spin Mapping Representation

Spin mapping maps a two-level quantum system onto a classical spin vector on a Bloch sphere by using the equivalence to a spin-1/2 particle in an external magnetic field (which is in a one-to-one correspondence with the Hamiltonian), as seen in Fig. 1.<sup>44</sup> The spin vector can then be propagated using Heisenberg's EOM,<sup>44,54</sup>

$$\dot{\mathbf{S}} = \mathbf{H} \times \mathbf{S}, \quad (25)$$



where,

$$\mathbf{S} = \begin{bmatrix} \sin \theta \cos \phi \\ \sin \theta \sin \phi \\ \cos \theta \end{bmatrix}. \quad (26)$$

The quantum-mechanical trace in the correlation function, Eqn. (1), is often calculated by using a Wigner transform,

$$A_W(q, p) = \int_{-\infty}^{\infty} dy e^{-\frac{i}{\hbar} py} \left\langle q + \frac{y}{2} \left| \hat{A} \right| q - \frac{y}{2} \right\rangle, \quad (27)$$

which maps the quantum operators onto a continuous phase-space such that the correlation function can be calculated with classical-like integrals. However, as the spin-vector is not continuous in the Hilbert space (as it is on the surface of the Bloch sphere) the Wigner transform cannot easily be utilised. Instead, the Stratonovich-Weyl transform is used which maps the operators onto a continuous function on the Lie group/manifold, which in the two state case is the surface of the sphere.<sup>44,49,51,54</sup> There are different transforms; known as Q-, P- and W-functions, which for two states result in radii of  $1/2$ ,  $3/2$  and  $\sqrt{3}/2$  respectively.<sup>44,54</sup> As the correlation functions tested here are written in the MMST formalism and we sample MMST variables prior to transforming into the spin-variables, we do not require the Stratonovich-Weyl transform explicitly.

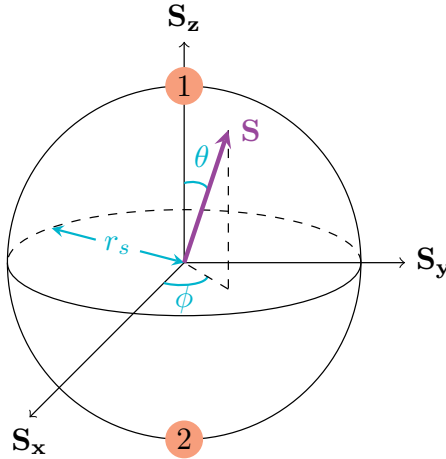


FIG. 1. The expectation values of the spin-operators form a basis of Cartesian coordinates where a Bloch sphere of radius,  $r_s$ , can be defined. The motion of the spin-vector (purple) on the surface is circular around the Hamiltonian vector. When the spin-vector is on either of the poles (orange circle), the population is entirely in one state.

The spin-mapping Hamiltonian is,<sup>44</sup>

$$H_{\text{SM}}(\mathbf{u}) = \frac{P^2}{2m} + V_0(R) + \frac{1}{2}\text{Tr}[\mathbf{V}] + \frac{1}{2}\mathbf{H} \cdot \mathbf{u}, \quad (28)$$

where,

$$\mathbf{H} = \begin{bmatrix} H_x \\ H_y \\ H_z \end{bmatrix} = \begin{bmatrix} \Delta^* + \Delta \\ i(\Delta^* - \Delta) \\ V_1 - V_2 \end{bmatrix}, \quad (29)$$

where we see that  $H_x$  is twice the real part of the coupling ( $\Delta$ ) and  $H_y$  is twice the imaginary part.

We define our scaled spin-vector as,

$$\mathbf{u} = \begin{bmatrix} u_x \\ u_y \\ u_z \end{bmatrix} = 2r_s \begin{bmatrix} S_x \\ S_y \\ S_z \end{bmatrix} = 2r_s \begin{bmatrix} \sin \theta \cos \phi \\ \sin \theta \sin \phi \\ \cos \theta \end{bmatrix}, \quad (30)$$

where  $r_s$  is the spin radius and the elements of  $\mathbf{S}$  are the spin-vector in Eqn. (26).<sup>44</sup> Hence, the spin-mapping Hamiltonian transforms as,

$$H_{\text{SM}}(\mathbf{u}) = \frac{P^2}{2m} + V_0(R) + \frac{1}{2}\text{Tr}[\mathbf{V}] + \frac{1}{2}(2\text{Re}(\Delta)u_x + 2\text{Im}(\Delta)u_y + (V_1 - V_2)u_z), \quad (31)$$

which is equivalent to the ZPE-Reduced MMST Hamiltonian, where  $\gamma = 2r_s - 1$ , due to the following coordinate transform for a two state system,<sup>44</sup>

$$u_x = q_1 q_2 + p_1 p_2, \quad (32a)$$

$$u_y = q_1 p_2 - q_2 p_1, \quad (32b)$$

$$u_z = \frac{1}{2}(q_1^2 + p_1^2 - q_2^2 - p_2^2), \quad (32c)$$

where  $\mathbf{q}$  and  $\mathbf{p}$  are canonical variables of the system and the spin-radius is,

$$4r_s = q_1^2 + p_1^2 + q_2^2 + p_2^2. \quad (33)$$

Several approaches for integrating the spin-mapping Hamiltonian have been proposed, these include converting into MMST variables to utilise one of the MMST algorithms<sup>44,49,66</sup> and the angle-based algorithm outlined in Appendix D which we later show is not symplectic.<sup>51,54,55</sup> Direct angle propagation can become unstable and hence, an algorithm extension has been developed where in these regions the elements of the spin-vector are directly propagated.<sup>55</sup> As far as we are aware, the only suggested symplectic scheme would be converting to the MMST representation and using the MInt algorithm.

### III. METHODOLOGY

We now present the Spin-MInt algorithm and its properties for the simplest possible nonadiabatic system of one nuclear and two electronic DoF. We extend the Spin-MInt algorithm to multiple nuclear and electronic states in Appendix E.<sup>49,51</sup>

#### A. Spin-MInt Algorithm

We split the spin-Hamiltonian into two sub-Hamiltonians,

$$H_{1,\text{SM}} = \frac{p^2}{2m}, \quad (34a)$$

$$H_{2,\text{SM}} = V_0(R) + \frac{1}{2}\text{Tr}[\mathbf{V}] + \frac{1}{2}\mathbf{H} \cdot \mathbf{u}, \quad (34b)$$

such that we can define the Spin-MInt algorithm with the following flow map,

$$\Psi_{H_{\text{SM}}, \Delta t}^{\text{Spin-MInt}} := \Phi_{H_{1,\text{SM}}, \frac{\Delta t}{2}} \circ \Phi_{H_{2,\text{SM}}, \Delta t} \circ \Phi_{H_{1,\text{SM}}, \frac{\Delta t}{2}}, \quad (35)$$

where only the integration of  $H_{2,\text{SM}}$ ,  $\Phi_{H_{2,\text{SM}}, \Delta t}$ , differs from the MInt algorithm as  $H_{1,\text{SM}} = H_{1,\text{MMST}}$ .<sup>66,68</sup> For  $H_{1,\text{SM}}$ , the evolution of  $R$  is identical to the MInt, Eqn. (8), and all other variables are unchanged.

For  $H_{2,\text{SM}}$ , the EOM follow from Eqn. (7) and Eqn. (25),

$$\dot{P} = -\mathbf{V}'_0(R) - \frac{1}{2}\text{Tr}[\mathbf{V}'(R)] - \frac{1}{2}\mathbf{H}' \cdot \mathbf{u}(t), \quad (36a)$$

$$\dot{u}_x = u_z H_y - u_y H_z, \quad (36b)$$

$$\dot{u}_y = -u_z H_x + u_x H_z, \quad (36c)$$

$$\dot{u}_z = u_y H_x - u_x H_y. \quad (36d)$$

For the electronic propagation, we can recast the cross product in Eqn. (25) as a matrix multiplication,

$$\dot{\mathbf{u}} = \begin{bmatrix} 0 & -H_z & H_y \\ H_z & 0 & -H_x \\ -H_y & H_x & 0 \end{bmatrix} \begin{bmatrix} u_x \\ u_y \\ u_z \end{bmatrix} \quad (37a)$$

$$= -i \begin{bmatrix} 0 & -i(V_1 - V_2) & \Delta - \Delta^* \\ i(V_1 - V_2) & 0 & -i(\Delta^* + \Delta) \\ -(\Delta - \Delta^*) & i(\Delta^* + \Delta) & 0 \end{bmatrix} \begin{bmatrix} u_x \\ u_y \\ u_z \end{bmatrix} \quad (37b)$$

$$= -i\mathbf{W}\mathbf{u}, \quad (37c)$$

where  $\mathbf{W}$  is Hermitian, skew-symmetric, and all elements are imaginary or zero. We could define this with an entirely real skew-symmetric matrix, but diagonalisation (which we later require) is only possible over the complex parts of a skew-symmetric matrix. Hence, we define  $\mathbf{W}$  to be  $i$  times the skew-symmetric matrix such that the diagonalisation is real.

We then integrate to obtain,

$$\mathbf{u}(t + \Delta t) = e^{-i\mathbf{W}\Delta t}\mathbf{u}(t), \quad (38)$$

which has the same form as the electronic propagation from the MInt algorithm,<sup>66,68</sup> Eqn. (10), except that  $\mathbf{W}$  is  $3 \times 3$  and  $\mathbf{V}$  is  $2 \times 2$ . This is a similar form to the spin-propagation of a time-reversible algorithm recently developed for MASH.<sup>61</sup> We note that as the MASH approach does not have a well-defined Hamiltonian, the Spin-MInt algorithm will not be applicable and symplectic propagation is unlikely to be obtained.<sup>45,61</sup>

We decompose  $\mathbf{W}$  into its eigenvalues and eigenvectors,

$$\mathbf{W} = \mathbf{S}_W \mathbf{\Lambda}_W \mathbf{S}_W^\dagger, \quad (39)$$

where as  $\mathbf{W}$  is Hermitian, the conjugate transpose, represented by  $\dagger$ , is the eigenvector inverse. The propagation is then,

$$\mathbf{u}(t + \Delta t) = \mathbf{S}_W e^{-i\mathbf{\Lambda}_W \Delta t} \mathbf{S}_W^\dagger \mathbf{u}(t). \quad (40)$$

The momentum integral in Eqn. (36a) integrates as,

$$P(\Delta t) = P(0) - \Delta t \left\{ \mathbf{V}'_0(R) + \frac{1}{2} \text{Tr}[\mathbf{V}'(R)] \right\} - \frac{1}{2} \int_0^{\Delta t} \mathbf{H}' \cdot e^{-i\mathbf{W}t} \mathbf{u}(0), \quad (41)$$

such that defining the last term as the integral,  $I_u$ , and using the decomposition in Eqn. (39) and inserting  $\mathbf{S}_W \mathbf{S}_W^\dagger$  identities,

$$I_u = \int_0^{\Delta t} \mathbf{H}' \mathbf{S}_W e^{-i\mathbf{\Lambda}_W t} \mathbf{S}_W^\dagger \mathbf{u}(0). \quad (42)$$

Element-wise integration results in,

$$I_u = \mathbf{H}' \mathbf{S}_W \mathbf{\Upsilon} \mathbf{S}_W^\dagger \mathbf{u}(0), \quad (43)$$

where,

$$\Upsilon_{nm} = \begin{cases} \frac{i}{\lambda_n}(e^{-i\lambda_n\Delta t} - 1) & n = m \text{ and } \lambda_n \neq 0 \\ \Delta t & n = m \text{ and } \lambda_n = 0 \\ 0 & n \neq m, \end{cases} \quad (44)$$

and  $\lambda_n$  is the eigenvalue. As  $\mathbf{W}$  is an odd-rank  $3 \times 3$  Hermitian matrix, one of the eigenvalues will be zero, and the other two are a  $\pm\lambda$  pair.

Overall, the integration of  $P$  is,

$$P(t + \Delta t) = P(t) - \Delta t \left( \mathbf{V}'_0 + \frac{1}{2}\text{Tr}[\mathbf{V}'] \right) - \frac{1}{2}\mathbf{H}'\mathbf{S}_W\mathbf{\Upsilon}\mathbf{S}_W^\dagger\mathbf{u}(t), \quad (45)$$

which can be implemented analytically. In Appendix B, we show that trajectories from the Spin-MInt propagation equations will be the same as with the MInt algorithm.

## B. Algorithm Steps

The Spin-MInt algorithm for the flow map in Eqn. (35) is,

1. Evolve nuclear position for  $\Delta t/2$  using Eqn. (8).
2. Calculate  $\mathbf{V}(R, \Delta t/2)$ ,  $\mathbf{V}_0(R, \Delta t/2)$  and derivatives with the updated nuclear position.
3. Calculate  $\mathbf{W}(R, \Delta t/2)$  from  $\mathbf{V}(R, \Delta t/2)$  and find  $\mathbf{S}_W$  and  $\mathbf{\Lambda}_W$  that diagonalise  $\mathbf{W}$ .
4. Evolve  $\mathbf{u}$  for  $\Delta t$  using Eqn. (38).
5. Use  $\mathbf{\Lambda}_W$  to calculate  $\mathbf{\Upsilon}$ . Find the derivative of  $\mathbf{H}$ .
6. Evolve nuclear momentum for  $\Delta t$  with Eqn. (45).
7. Repeat step 1 for the second half-timestep of  $H_1$ .

such that repeating for  $N$  timesteps results in a simulation of length  $N\Delta t$  time units.

## C. Spin-MInt Properties

We wish to prove that the Spin-MInt algorithm is a symplectic, symmetric, second-order, time-reversible, angle invariant and structure preserving method.

## 1. Symmetric and Second-Order

A symmetric algorithm is defined as  $(\Psi_{\Delta t})^{-1} = \Psi_{-\Delta t}$ .<sup>67,68</sup> As exact evolution under any Hamiltonian or sub-Hamiltonian is symmetric,<sup>67,68</sup> and  $\Psi_{H_{SM}, \Delta t}^{\text{Spin-MInt}}$  is a symmetric composition of exact sub-Hamiltonian evolutions (where  $H_1$  is symmetrically split around  $H_2$ ), we immediately see that  $\Psi_{H_{SM}, \Delta t}^{\text{Spin-MInt}}$  is symmetric.

A second-order method has a flow map that deviates from the exact solution on order  $(\Delta t)^2$ .<sup>68</sup> Using the same reasoning as for the MInt algorithm,<sup>68</sup> a symmetric method necessarily has even order and a symplectic method has order greater than or equal to 1. Thus, the Spin-MInt must be at least second order.

## 2. Symplecticity

We can infer symplecticity of the Spin-MInt algorithm from the evolution equations being equivalent to the MInt and therefore, the algorithm is a composition of exact sub-Hamiltonian integrations and will be symplectic for any number of electronic states.<sup>66–68</sup>

To rigorously prove symplecticity, we need to define a structure matrix for the spin-variables such that we can evaluate the symplecticity criterion in Eqn. (22). We can describe a Hamiltonian system with Eqn. (20), where  $\mathbf{z}^T = [R, P, u_x, u_y, u_z]$ . However, as the spin-variables are evolved with Heisenberg's EOM, Eqn. (25), the structure matrix would be,

$$\mathbf{J} = \begin{bmatrix} 0 & 1 & \mathbf{0} \\ -1 & 0 & \mathbf{0} \\ \mathbf{0}^T & \mathbf{0}^T & \mathbf{K} \end{bmatrix}, \quad (46)$$

where,  $\mathbf{0} = [0, 0, 0]$  and,

$$\mathbf{K} = \begin{bmatrix} 0 & u_z & -u_y \\ -u_z & 0 & u_x \\ u_y & -u_x & 0 \end{bmatrix}, \quad (47)$$

which is the spin-rotation matrix. However,  $\mathbf{K}$  is singular and non-invertible, due to non-canonical spin-variables. Hence, the full structure matrix, Eqn. (46), is also non-invertible which makes evaluating the symplecticity criterion challenging.

Whilst previous work has suggested defining a non-canonically symplectic integrator, or more commonly referred to as a Poisson integrator, as one that is structure preserving where the spin-magnitude is conserved throughout simulation.<sup>75,80</sup> In section III C 4, we show that this is not sufficient to prove symplecticity when there is non-trivial coupling between canonical and spin systems. We would like to prove that this algorithm is symplectic in a more rigorous manner.

In Ref. [54], the idea of canonical conjugate variables to re-obtain Hamilton's EOM is discussed. These conjugate variables are,

$$\dot{\phi} = \frac{\partial H_{2,SM}}{\partial r_s \cos \theta}, \quad (48a)$$

$$r_s \dot{\cos \theta} = -\frac{\partial H_{2,SM}}{\partial \phi}, \quad (48b)$$

which results in the structure matrix,

$$\mathbf{J} = \begin{bmatrix} \mathbb{O} & \mathbb{I} \\ -\mathbb{I} & \mathbb{O} \end{bmatrix}, \quad (49)$$

which is the same as the MMST representation, Eqn. (21), in the  $4 \times 4$  form. The system is then described by  $\mathbf{z}^T = [R, \phi, P, r_s \cos \theta]$  such that the monodromy matrix is,

$$\mathbf{M}_{SM} = \begin{bmatrix} M_{RR} & M_{R\phi} & M_{RP} & M_{Rr_s \cos \theta} \\ M_{\phi R} & M_{\phi\phi} & M_{\phi P} & M_{\phi r_s \cos \theta} \\ M_{PR} & M_{P\phi} & M_{PP} & M_{Pr_s \cos \theta} \\ M_{r_s \cos \theta R} & M_{r_s \cos \theta \phi} & M_{r_s \cos \theta P} & M_{r_s \cos \theta r_s \cos \theta} \end{bmatrix}. \quad (50)$$

We define the monodromy matrix elements for the Spin-MInt algorithm in Appendix C. In Section IE of the Supplementary Material, we show this matrix satisfies Liouville's theorem ( $|\mathbf{M}| = 1$ ) which results in phase-space preservation. In Section ID of the Supplementary Material, we define an explicit version of the monodromy matrix for two states where  $H_y = 0$ , which is equivalent to the form in Appendix C but challenging to generalise for more than two electronic states. Whilst we can infer symplecticity from the exact sub-Hamiltonian evolution, we algebraically prove symplecticity in Section IF of the Supplementary Material for two states with  $H_y = 0$  using the explicit form of the monodromy matrix.

The Spin-MInt is therefore, to the best of our knowledge, the first known symplectic algorithm for a spin-mapping Hamiltonian and we have rigorously prove symplecticity despite a non-invertible spin-variable structure matrix via a canonical coordinate transform.

### 3. Time-Reversible

A method with flow map  $\Psi$  is time-reversible (under an involution  $\Sigma$ ) if  $\Psi = \Sigma\Psi^{-1}(\Sigma\mathbf{z})$ .<sup>67,68</sup> To determine the form of the involution matrix, we first investigate the time-reversal behaviour of the variables,  $\mathbf{z}^T = [R, \phi, P, r_s \cos \theta]$ .

Trivially,  $R$  is unchanged under time-reversal and  $P \mapsto -P$ . We note that  $u_z = 2r_s \cos \theta$  and  $\tan(\phi) = u_x/u_y$ . Using the transformation in Eqn. (32), we see that  $u_x$  and  $u_z$  are unchanged due to the even  $p$  term order. Hence,  $r_s \cos \theta$  is unchanged under time-reversal. As  $u_y \mapsto -u_y$ ,  $\tan(\phi) \mapsto -\tan(\phi)$  and as  $\tan$  is an odd function results in  $\phi \mapsto -\phi$ . The involution matrix is then,

$$\Sigma = \begin{bmatrix} 1 & 0 & 0 & 0 \\ 0 & -1 & 0 & 0 \\ 0 & 0 & -1 & 0 \\ 0 & 0 & 0 & 1 \end{bmatrix}. \quad (51)$$

Since  $H_{2,\text{SM}}(R, \phi, P, r_s \cos \theta) = H_{2,\text{SM}}(R, -\phi, -P, r_s \cos \theta)$ , evolution under this sub-Hamiltonian will be time-reversible, and  $H_{1,\text{SM}}$  is time-reversible.<sup>68</sup> Therefore, the Spin-MInt is a time-reversible algorithm as these evolution maps are composed symmetrically.

### 4. Structure Preservation and Angle Invariance

We can show that the Spin-MInt algorithm preserves the geometric structure of the Poisson bracket by preserving the Casimirs' of the bracket,<sup>75,81</sup> which results in conservation of the magnitude of  $\mathbf{u}$  and further details are found in Ref. [49]. The spin-vector is evolved under Eqn. (38) such that the transformation is,

$$\mathbf{T} = e^{-i\mathbf{W}t}, \quad (52)$$

where as  $\mathbf{W}$  is Hermitian, the transformation matrix is unitary. The norm of the spin vector is preserved as,

$$||\mathbf{T}\mathbf{u}||^2 = (\mathbf{T}\mathbf{u})^\dagger(\mathbf{T}\mathbf{u}) = ||\mathbf{u}||^2, \quad (53)$$

such that,  $\langle \mathbf{u} | \mathbf{u} \rangle$  is conserved. We show this numerically in the Supplementary Material Figure S.9. We note that structure preservation is a weaker criteria than symplecticity, as one can derive a structure preserving but not symplectic spin-mapping algorithm utilising a Split-Liouillian (SL)



formalism. We algebraically show this in the Supplementary Material Section IG where we obtain a structure preserving electronic evolution but not an exact sub-Hamiltonian  $H_{2,\text{SM}}$  evolution.

Structure preservation also results in an invariance to the overall phase of the spin-vector. A phase-space transformation is described by,

$$\tilde{\mathbf{u}} = e^{-i\theta} \mathbf{u}, \quad (54)$$

which commutes with  $\mathbf{T}$  for any scalar  $\theta$ . Therefore, the spin-vector evolution is unaffected by any angle shift using Eqn. (54) and back again.

## IV. RESULTS

For algorithmic comparison, we utilise the same models used in Ref. [66] to extend our benchmarking to spin-mapping algorithms using one nuclear and two electronic DoF.<sup>28</sup> These models are for a one-dimensional spin-boson model where the diabatic potential matrix is,

$$\tilde{\mathbf{V}} = \mathbf{V}_0 + \mathbf{V} \quad (55)$$

$$= \frac{1}{2} m \omega^2 x^2 \mathbb{I} + \begin{bmatrix} \alpha + \kappa x & \Delta \\ \Delta & -\alpha - \kappa x \end{bmatrix}, \quad (56)$$

where we have split into a traceless state-dependent matrix,  $\mathbf{V}$ , and a state-dependent matrix,  $\mathbf{V}_0$ . We note that neither algorithm requires a traceless  $\mathbf{V}$  matrix and we use this model to allow literature comparison.<sup>66</sup> We utilise reduced units where  $m = \hbar = \omega = 1$ . There are three models with different values of electronic coupling,  $\Delta$  and energy bias,  $\alpha$ , outlined in Table I. In all three models we choose the vibronic coupling,  $\kappa = 1$ .<sup>66</sup> Model 1 is in the adiabatic limit where there is strong electronic coupling. Model 2 is in the inverted Marcus regime where there is a large energy bias between surfaces. Model 3 is an intermediate regime which is the most challenging to simulate due to similar timescales of electronic and nuclear dynamics.<sup>66</sup>

Model	$\alpha$	$\Delta$
1	0	4
2	2	1
3	0	1

TABLE I. Values for the potential matrix constants for Models 1-3 from Refs. [28,66].

We use the same distribution and sampling as outlined in Appendix D of Ref. [66]. We sample the electronic  $\mathbf{q}$  and  $\mathbf{p}$  and transform this into the  $\mathbf{u}$  vector for propagation with the Spin-MInt algorithm or angles  $\theta$  and  $\phi$  for the angle-based algorithm outlined in Appendix D. This ensures that we can compare the algorithms as the starting variables are equivalent and the same sampling is used for ensemble calculations. It is easier to convert from  $\mathbf{q}$  and  $\mathbf{p}$  into the spin-variables as there is a larger number of MMST variables compared to either spin-representation. We use the single-bead form of the NRPMD distribution,<sup>28,66</sup>

$$\rho = \frac{4}{\pi^2} e^{-|\mathbf{q}^2| - |\mathbf{p}^2| - \beta(\mathbf{V}_0 + P^2/2m)}, \quad (57)$$

such that the partition function is

$$Z = \langle Q \rangle_\rho, \quad (58)$$

where  $Q = \mathbf{p}^T e^{-\beta \mathbf{V}/2} \mathbf{q} \times \mathbf{q}^T e^{-\beta \mathbf{V}/2} \mathbf{p}$  is the weighting (positive definite for a single bead).

### A. Single Trajectory Comparison

For a single trajectory, we compare the accuracy of the Spin-MInt algorithm against the MInt algorithm and an angle-based algorithm from Ref. [54].<sup>54,68</sup> The angle-based algorithm directly propagates  $\theta$  and  $\phi$  and is outlined in Appendix D.<sup>51,54</sup> In Figure 2, we show the propagation of  $u_x$  using the three algorithms. We find that a small timestep is required to obtain accurate propagation using the angle-based algorithm. However, the Spin-MInt and MInt algorithms are much more tolerant of a large timestep, capturing the correct dynamics at all timesteps in Figure 2. The Spin-MInt and MInt algorithms are identical in propagation, as seen in the SI for nuclear and electronic variables with all three models (Figure S.1-S.6).

It has been noted in the literature that when  $\theta \rightarrow 0, n\pi$ , angle-based algorithms are likely to become unstable and swapping to propagation of the spin-vector is advised.<sup>51,54</sup> However, as this makes computing the monodromy matrix complicated, to compare the symplecticity and satisfaction of Liouville's theorem, we focus on trajectories that do not reach these unstable regions. In Figure 3, we present the symplecticity criterion and satisfaction of Liouville's theorem for the trajectory in Figure 2 using Model 1 with  $\Delta t = 0.1$ .

To compare the symplecticity, we evaluate the symplecticity criterion by defining an error matrix,<sup>66</sup>

$$\mathbf{E}_r = \mathbf{M}^T \mathbf{J}^{-1} \mathbf{M} - \mathbf{J}^{-1}, \quad (59)$$

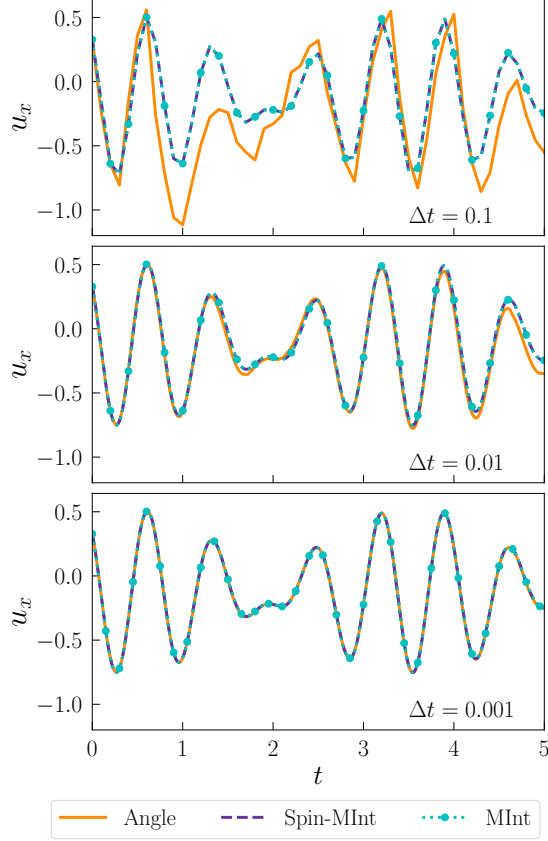


FIG. 2. Propagation of  $u_x$  for a single trajectory using Model 1 and the MInt (cyan dotted circles), Spin-MInt (purple dashed) and angle-based (orange) algorithms at three different timesteps: 0.1 (top), 0.01 (middle) and 0.001 (bottom). The Spin-MInt and MInt results are identical at all timesteps whilst the angle-based algorithm deviates for the 0.1 and 0.01 timesteps indicating lower accuracy.

where for a symplectic integrator the elements of  $\mathbf{E}_r$ ,  $e_{ij}$ , will be zero.<sup>74</sup> We then utilise the Frobenius Norm to track the size of the error matrix,<sup>66</sup>

$$\|\mathbf{E}_r\|_F = \sqrt{\sum_{i=1}^n \sum_{j=1}^n |e_{ij}|^2}, \quad (60)$$

where the matrix size is  $n \times n$ .<sup>74</sup> In Figure 3 (a), we show a logarithmic plot of  $\|\mathbf{E}_r\|_F$  against time for the single trajectory in Figure 2. The Spin-MInt (purple) and MInt (cyan) algorithms remain below  $10^{-12}$  for the whole trajectory and therefore are symplectic. However, the angle-based algorithm (orange) rapidly increases to the order of  $10^{-1}$ , indicating lack of symplecticity.

We can define two mathematically identical ways of implementing the Spin-MInt algorithm for the two-state potential tested in Eqn. (55). To calculate  $e^{-i\mathbf{W}t}$ , one can decompose into eigenvalues and eigenvectors (resulting in the monodromy matrix in Appendix C) or through an explicit form

outlined in the Supplementary Material Section ID. In Figure S.8 of the Supplementary Material, we show that the explicit form of the monodromy matrix results in lower floating point error. However, this explicit form is not easily extendable to more than two states such that we use the decomposition method and the monodromy in Appendix C here.

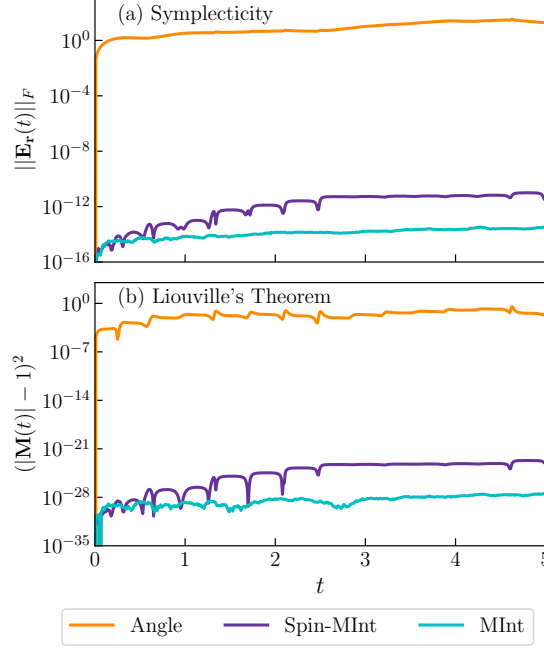


FIG. 3. (a) The error matrix Frobenius norm and (b) the Liouville's theorem criterion as a function of time using Model 1 and  $\Delta t = 0.01$ , for a single trajectory using the Spin-MInt (purple), MInt (cyan) and angle-based (orange) algorithms. As the MInt and Spin-MInt algorithms measure floating point error in both plots, Liouville's theorem and symplecticity are satisfied. The angle-based algorithm does not satisfy symplecticity or Liouville's theorem.

To evaluate satisfaction of Liouville's theorem, where  $|\mathbf{M}| = 1$ ,<sup>66,82,83</sup> we plot  $(|\mathbf{M}| - 1)^2$  in Figure 3 (b). We see that the Spin-MInt and MInt algorithms satisfy Liouville's theorem. The angle-based algorithm does not satisfy Liouville's theorem as the orange line is not within floating point error which is uncommon for a mapping algorithm.<sup>66</sup> From the algebraic monodromy in Appendix D, it is clear that the determinant will initially deviate from unity on  $\mathcal{O}(\Delta t)$  as in Eqn. (D.5) such that it is zero order with respect to timestep when propagating for a given length of time.<sup>66</sup> In the Supplementary Material Figure S.7 we see that a smaller timestep does not improve the satisfaction of Liouville's theorem.

For a single trajectory, the Spin-MInt and MInt algorithms result in the same propagation of

variables and are both symplectic. As the angle-based algorithm is not symplectic or satisfies Liouville's theorem and requires a small timestep to accurately capture the dynamics, we do not consider it further in our search for a symplectic spin-mapping algorithm.

## B. Ensemble Properties

To test the ensemble properties, we define the same criteria as in Ref. [66] and weight by  $Q$ ,<sup>66</sup>

$$\langle \|\mathbf{E}_r\|_F \rangle_\rho = \frac{\sum_{i=1}^J (\|\mathbf{E}_r\|_F)_i(t) Q_i(0)}{\sum_{i=1}^J Q_i(0)}, \quad (61)$$

where  $i$  is the trajectory index. For Liouville's theorem, we evaluate

$$\langle (|\mathbf{M}| - 1)^2 \rangle_\rho = \frac{\sum_{i=1}^J (|\mathbf{M}_i(t)| - 1)^2 Q_i(0)}{\sum_{i=1}^J Q_i(0)}, \quad (62)$$

where we square the deviation to ensure no error cancellation.<sup>66</sup> Satisfying Liouville's theorem does not always indicate an accurate algorithm as it is equivalent to having a divergenceless

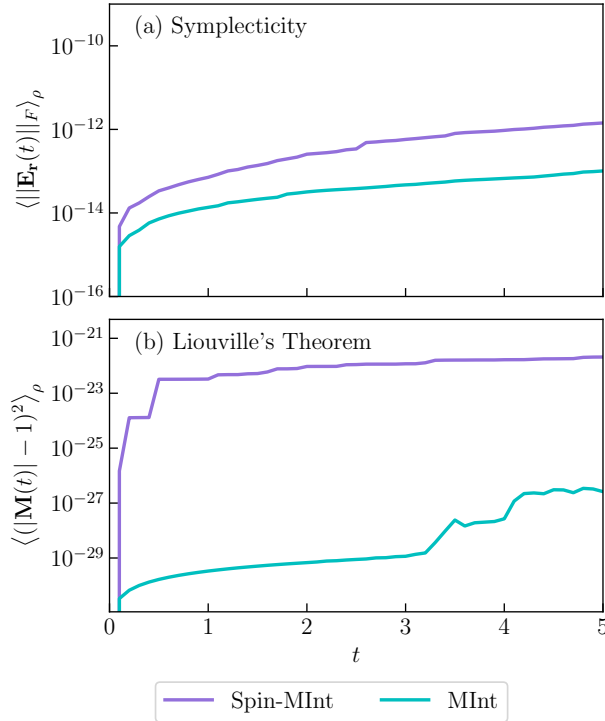


FIG. 4. (a) The error matrix Frobenius norm and (b) the Liouville's theorem criterion as a function of time using Model 1 and  $\Delta t = 0.1$ , averaged over a million trajectories using the Spin-MInt (purple) and MInt (cyan) algorithms. In (a) the algorithms are symplectic and in (b) the algorithms satisfy Liouville's theorem as both plots measure floating point errors.

Liouvillian.<sup>66,84</sup> However, as the MInt algorithm does satisfy this,<sup>66</sup> we wish to prove this for the Spin-MInt.

In Figure 4a, we present the logarithmic plot of  $\|\mathbf{E}_r\|_F$  against time for Model 1 with  $\Delta t = 0.1$ . Both algorithms remain below  $10^{-12}$ , with a small build up of floating-point errors,<sup>66</sup> for the entire simulation time. Both algorithms are therefore symplectic.<sup>66,68</sup> In Figure 4b, we see that both algorithms satisfy Liouville's theorem and conserve volume phase-space.

For energy conservation, the criterion is,<sup>66</sup>

$$\langle (\epsilon(t) - \epsilon(0))^2 \rangle_\rho = \frac{\sum_{i=1}^J (\epsilon(t) - \epsilon(0))^2 Q_i(0)}{\sum_{i=1}^J Q_i(0)}, \quad (63)$$

where the energy,  $\epsilon$ , is calculated by evaluating the Hamiltonians, Eqn (3) and Eqn. (31) for the

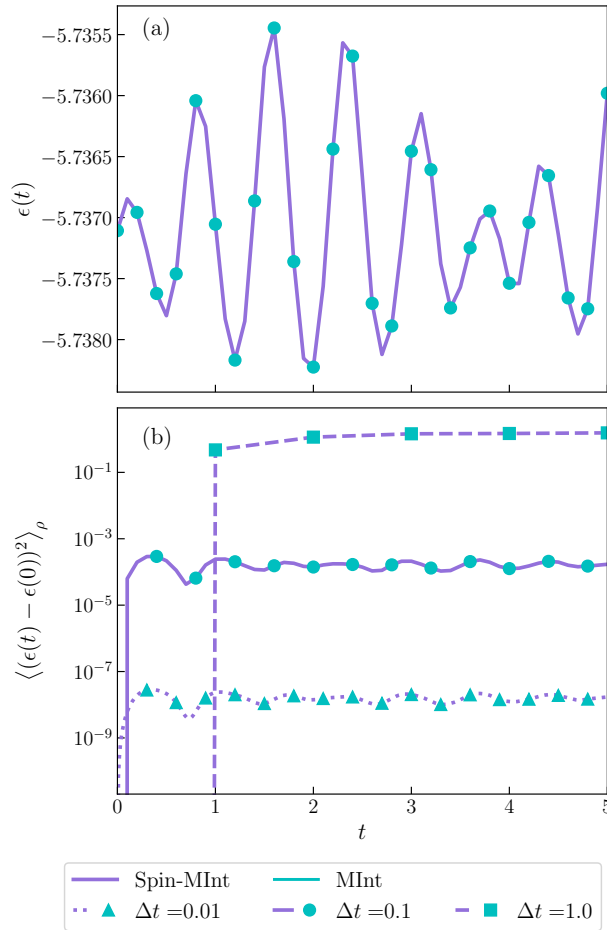


FIG. 5. Energy conservation of Model 1 with (a) a single trajectory and  $\Delta t = 0.1$  (solid/circle) and (b) averaged using  $\Delta t = 0.1$  (solid/circle),  $\Delta t = 0.01$  (dotted/triangle) and  $\Delta t = 1.0$  (dashed/square) with the Spin-MInt (purple) and MInt (cyan) algorithms. The energy is the same for both algorithms and is conserved by noting the y-axis scale on (a) and is second-order with respect to timestep in (b).

MInt and Spin-MInt algorithms respectively, at each timestep.<sup>66</sup>

In Figure 5, we plot the energy conservation for (a) a single trajectory and (b) an ensemble of trajectories. We see that the Spin-MInt and MInt algorithms both conserve energy for a single trajectory, noting the very small oscillations in (a), and for an ensemble of trajectories. For the ensemble, both algorithms are easily shown to be second-order as changing the timestep by a factor of 10 results in a change of  $10^4$  in the energy criterion.<sup>66</sup> This agrees with the algebraic determination of order for the MInt in Ref. [68] and the derivation in Section III C for the Spin-MInt.<sup>68</sup> For a symplectic algorithm, this means the energy of the approximate Hamiltonian is exactly conserved which differs from the exact Hamiltonian by the order of the algorithm,<sup>66–68</sup> resulting in energy conservation at exponentially long-times with fluctuations on  $\mathcal{O}(\Delta t^2)$ .<sup>66</sup>

The corresponding energy conservation for Models 2 and 3 are included in the Supplementary Material (Figures S.10 and S.11) as well as structure preservation resulting in spin-magnitude conservation for the Spin-MInt in Figure S.9.

### C. Correlation Functions

To approximate the correlation functions in Eqn. (1), we calculate the following where for the position auto-correlation function  $\hat{A} = \hat{B} = R$  and for the population auto-correlation function  $\hat{A} = A_n$  and  $\hat{B} = B_n$ ,<sup>66</sup>

$$\tilde{C}_{RR}(t) \simeq \frac{\langle R(0) R(t) Q \rangle_\rho}{\langle Q \rangle_\rho}, \quad (64a)$$

$$\tilde{C}_{nn}(t) \simeq \frac{\langle A_n(0) B_n(t) Q \rangle_\rho}{\langle Q \rangle_\rho}, \quad (64b)$$

where  $Q(\mathbf{q}(0), \mathbf{p}(0))$  and initial conditions are sampled as outlined in Ref. [66], specifically Eqn. (D.14) for  $J$  trajectories. Averaging over trajectories results in,

$$\tilde{C}_{RR}(t) = \frac{\sum_{i=1}^J R_i(0) R_i(t) Q_i(0)}{\sum_{i=1}^J Q_i(0)}, \quad (65a)$$

$$\tilde{C}_{nn}(t) = \frac{\sum_{i=1}^J A_{ni}(0) B_{ni}(t) Q_i(0)}{\sum_{i=1}^J Q_i(0)}, \quad (65b)$$

where index  $i$  refers to the  $i$ -th trajectory. The initial electronic state population is defined as,<sup>66,71</sup>

$$A_n = \frac{p_n [e^{-\beta \mathbf{V}/2} \mathbf{q}]_n}{\mathbf{p}^T e^{-\beta \mathbf{V}/2} \mathbf{q}}, \quad (66)$$

where as we sample  $\mathbf{q}$  and  $\mathbf{p}$  before transforming into spin-mapping variables, we do not need to define this in terms of  $\mathbf{u}$ . The electronic populations at time  $t$  are,<sup>71</sup>

$$B_{n,\text{MMST}} = \frac{1}{2} (X_n(t)^2 + P_n(t)^2 - 1), \quad (67)$$

for the MInt algorithm and, for the Spin-MInt algorithm with two electronic states

$$B_{1,\text{SM}} = r_s + \frac{1}{2}(u_z - 1), \quad (68a)$$

$$B_{2,\text{SM}} = r_s - \frac{1}{2}(u_z + 1). \quad (68b)$$

We present the correlation functions in Figure 6 for all three models tested. We see that the Spin-MInt and MInt algorithm reproduce the same correlation functions, as expected from the equivalent propagations. Previous work has shown that the MInt algorithm produces accurate correlation functions and the results here agree with the literature.<sup>66,71</sup> In Model 1, we see the fast oscillations in the electronic population auto-correlation function as expected from a system close to the adiabatic limit, indicating that the electronic dynamics are on much faster timescale than the

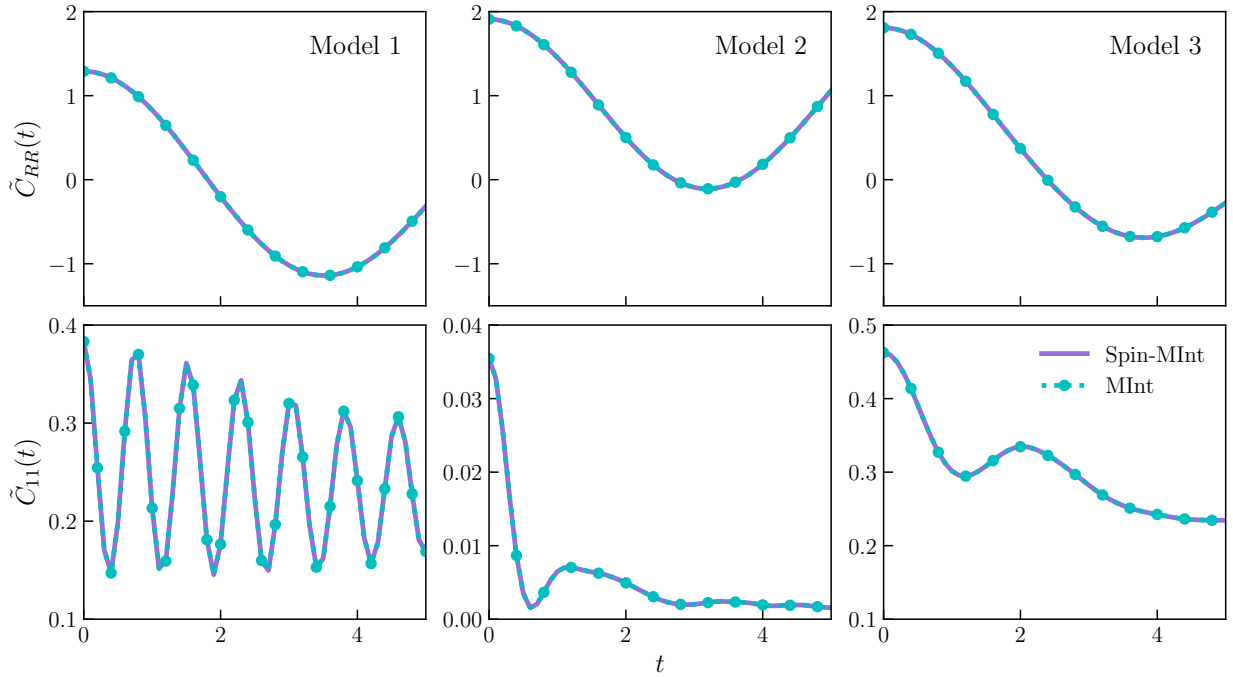


FIG. 6. The nuclear position,  $\tilde{C}_{RR}(t)$ , and electronic population,  $\tilde{C}_{11}(t)$ , autocorrelation functions for Models 1, 2 and 3 using  $\Delta t = 0.1$  with the Spin-MInt (purple solid) and MInt (cyan dotted circle) algorithms. Both algorithms result in the same correlation functions and agree with the literature.<sup>66</sup>



nuclear dynamics. The energy bias in Model 2 results in a fast equilibrium forming, which is seen as a loss of population in the first electronic state.<sup>66,71</sup> For Models 2 and 3, there is weak coupling which results in slower oscillations. However, Model 3 is the most challenging to simulate due to the additional lack of energy bias. Therefore, the Spin-MInt accurately captures the dynamics in the same way the MInt algorithm does.

#### D. Three State Results

In Appendix E, we generalise the Spin-MInt algorithm to multiple electronic and nuclear states. Here, we model a three state system with one nuclear DoF, a Morse potential model,<sup>51,85</sup> with the potential matrix,

$$V_{ii} = D_{ii} \left( 1 - e^{-\alpha_{ii}(R-R_{ii})} \right)^2 + c_{ii}, \quad (69a)$$

$$V_{ij} = A_{ij} e^{-\alpha_{ij}(R-R_{ij})^2}, \quad (69b)$$

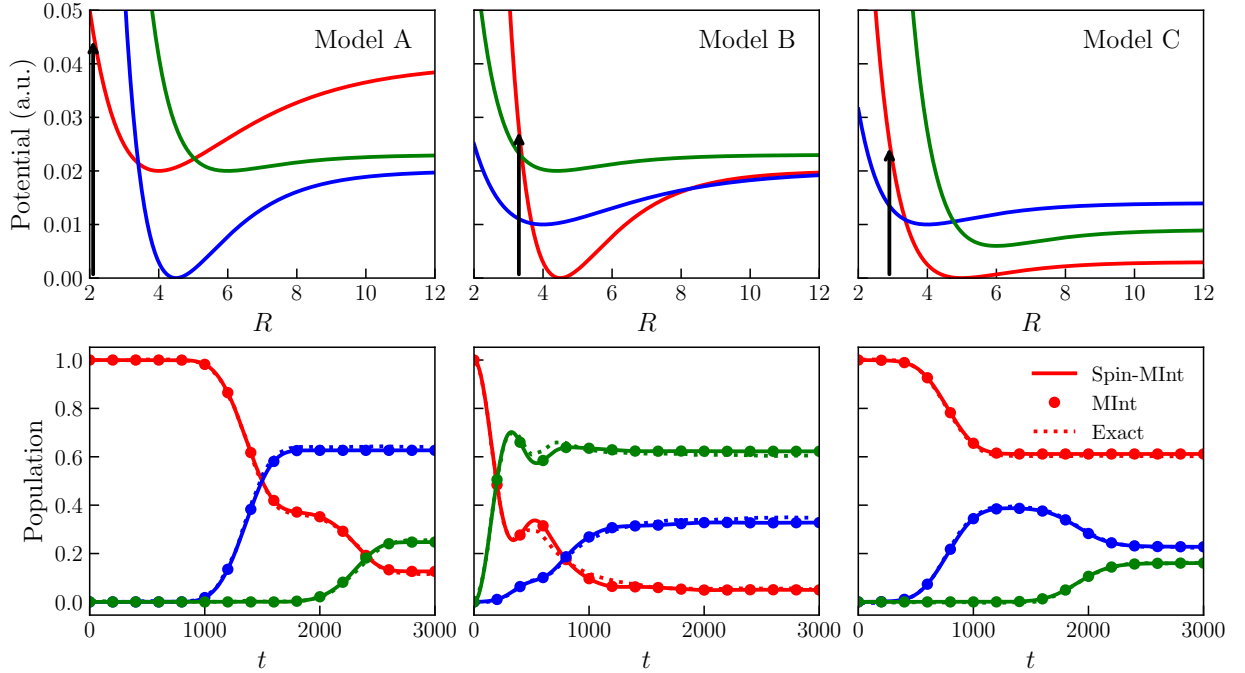


FIG. 7. Three state Morse potential results for Models A, B and C with the diabatic potential energy surfaces (top row) and state populations (bottom row). Focused initial conditions are prepared on the first state (red) at the vertical arrows. Parameters are in Table S.2 in the Supplementary Material. The MInt (circles) and Spin-MInt (solid line) result in identical population dynamics that agree closely with the exact result from literature (dotted).<sup>51,85</sup>

where we have three models (A/B/C) with tabulated parameters in the Supplementary Material (Table S.2), and we focus the initial sampling on the first state as detailed in Section II of the Supplementary Material.

In Figure 7, we plot the population dynamics of the three states, calculated using,

$$\mathcal{P}_{n,\text{MMST}} = \frac{1}{2} (q_n^2 + p_n^2 - \gamma), \quad (70)$$

for the MMST representation where for  $N$  electronic states,  $\gamma = 2(r_s - 1)/N$  and,

$$\mathcal{P}_{n,\text{SM}} = \frac{1}{N} + r_s \left[ \sum_{m=n+1}^N \left( \sqrt{\frac{2}{m(m+1)}} \Omega_{\gamma_m} \right) - \sqrt{\frac{2(n-1)}{n}} \Omega_{\gamma_n} \right], \quad (71)$$

for the spin-mapping representation where  $\Omega$  is defined in Eqn (E.9). We see that these results agree with previous literature,<sup>51,85</sup> and conclude that the generalised Spin-MInt algorithm is accurate. The results here were calculated using a 1.0 timestep and  $10^5$  trajectories. For Models B/C,  $5 \times 10^5$  trajectories were required in the literature,<sup>51</sup> so the Spin-MInt algorithm provides faster convergence of these results.

## E. Computational Timings

In Table S.3 of the Supplementary Material, we present computational timings for the MInt (both in MMST variables and transforming into spin-mapping variables) and Spin-MInt algorithms using the two and three state models discussed. We find a significant speed up using the Spin-MInt for the two-level system compared to the MInt algorithm, which motivates utilisation of this algorithm for two-level spin-mapping systems. In comparison to previous work,<sup>66</sup> this implementation of the MInt is faster due to the ordering of sub-Hamiltonian propagation in the flow map, Eqn. (6), which has a lower computational cost.<sup>68</sup> However, for larger systems, the Spin-MInt has poorer scaling than the MInt, likely due to the  $N^2 - 1$  spin-mapping vector compared to  $2N$  variables for the MMST representation. Despite this, a faster implementation may be possible and direct sampling of the spin-mapping variables is likely to lower the associated generalised Spin-MInt computational cost.

## V. CONCLUSIONS

We have presented the first known symplectic algorithm for propagation of the spin-vector using the spin-mapping Hamiltonian. Whilst previous work has assumed structure preservation

results in symplecticity, we have shown this is not sufficient for the non-trivial coupling between the canonical nuclear and electronic spin systems through a Split-Liouvillian formalism (Supplementary Material Section IG). Instead, we have rigorously proven symplecticity (Supplementary Material Section IF) when the structure matrix is non-invertible by defining the monodromy matrix in conjugate canonical variables. The Spin-MInt provides the same evolution as the MInt algorithm, shown both algebraically (Appendix B) and numerically (Figure 2).

For a two-state model, we compared single trajectories to the MInt algorithm and an angle-based algorithm.<sup>54,66,68</sup> The angle-based algorithm required small timesteps to accurately propagate the variables and is not symplectic or satisfies Liouville’s theorem, in contrast to the Spin-MInt and MInt algorithms which satisfy all these criteria. Hence, we did not consider the angle-based algorithm further. For an ensemble, we find that the Spin-MInt and MInt algorithm accurately capture the correlation functions,<sup>66</sup> satisfy Liouville’s theorem, are symplectic and have second-order energy conservation. The Spin-MInt is also structure preserving, although this is a weaker condition than symplecticity.

We have generalised the Spin-MInt algorithm to multiple nuclear and electronic states using the spin coherent states from the literature.<sup>49,51</sup> For a three-state Morse potential, we accurately capture the population dynamics with fewer trajectories than required using an angle-based algorithm in the literature.<sup>51</sup> We find that the Spin-MInt algorithm is significantly faster than the MInt for the two-level system but seems to have poorer scaling with more electronic states. However, a faster implementation may be possible, especially if sampling spin-mapping variables as opposed to MMST variables and converting. This algorithm should be utilised in future spin-mapping simulations to ensure accurate and symplectic propagation without the additional cost of variable transformation.

## SUPPLEMENTARY MATERIAL

The supplementary material comprises of three sections; additional algebra, the three-state model and additional results. The additional algebra section includes decomposition of  $\mathbf{V}$  and  $\mathbf{W}$  when  $\Delta$  is real, an alternative Spin-MInt nuclear momentum propagation, an explicit form of  $e^{-i\mathbf{W}t}$  and related integral and derivatives when  $\Delta$  is real, proof of satisfaction of Liouville’s theorem and symplecticity for the Spin-MInt algorithm, and a Split-Liouvillian spin algorithm. The three-state model section tabulates model parameters and details the sampling. The additional results section

consists of further two-state single trajectory (variable propagation and symplecticity at different timesteps), ensemble trajectory results (spin-magnitude and energy conservation) and tabulated computational timings.

## ACKNOWLEDGEMENTS

TJHH acknowledges a Royal Society University Research Fellowship URF\R1\201502. LEC acknowledges a University College London studentship. JRR acknowledges a summer studentship funded by TJHH's RS URF and funding from the Engineering and Physical Sciences Research Council [grant number EP/Z534882/1]. We thank Pengfei (Frank) Huo and Duncan Bossion for sharing details of the angle-based algorithm.

## AUTHOR DECLARATION

The authors have no conflicts to disclose.

## DATA AVAILABILITY

The data that support the findings of this study are openly available in UCL Research Data Repository at [http://doi.org/\[to be inserted\]](http://doi.org/[to be inserted]), reference number [to be inserted].

## APPENDICES

### A. MInt Monodromy Matrices

For the MMST variable system, the monodromy matrix is,<sup>66,68</sup>

$$\mathbf{M} = \begin{bmatrix} \mathbf{M}_{RR} & \mathbf{M}_{Rq} & \mathbf{M}_{RP} & \mathbf{M}_{Rp} \\ \mathbf{M}_{qR} & \mathbf{M}_{qq} & \mathbf{M}_{qP} & \mathbf{M}_{qp} \\ \mathbf{M}_{pR} & \mathbf{M}_{pq} & \mathbf{M}_{pP} & \mathbf{M}_{pp} \end{bmatrix}, \quad (\text{A.1})$$

such that the monodromy matrix for  $H_{1,\text{MMST}}$  using the MInt is

$$\mathbf{M}_{\text{M},H_{1,\text{MMST}}} = \begin{bmatrix} 1 & \mathbf{0}^T & \frac{\Delta t}{M} & \mathbf{0}^T \\ \mathbf{0} & \mathbb{I} & \mathbf{0} & \mathbb{O} \\ 0 & \mathbf{0}^T & 1 & \mathbf{0}^T \\ \mathbf{0} & \mathbb{O} & 0 & \mathbb{I} \end{bmatrix}, \quad (\text{A.2})$$

where  $\mathbf{0}^T = [0, 0]$ , the determinant is unity,  $|\mathbf{M}_{\text{M},H_{1,\text{MMST}}}| = 1$  and satisfies the symplecticity criterion in Eqn. (22).<sup>66,68</sup>

The monodromy matrix for  $H_{2,\text{MMST}}$  can be found by defining,

$$\mathbf{a} = -\mathbf{p}^T \mathbf{E} + \mathbf{q}^T \mathbf{F}, \quad (\text{A.3a})$$

$$b = -\Delta t \mathbf{V}_0'' - \frac{1}{2} (\mathbf{q}^T \mathbf{E}' \mathbf{q} + \mathbf{p}^T \mathbf{E}' \mathbf{p} - 2\mathbf{q}^T \mathbf{F}' \mathbf{p}) + \frac{1}{2} \text{Tr}[\mathbf{V}''] \Delta t, \quad (\text{A.3b})$$

$$\mathbf{e} = -\mathbf{q}^T \mathbf{E} - \mathbf{p}^T \mathbf{F}, \quad (\text{A.3c})$$

$$\mathbf{f} = \mathbf{C}' \mathbf{p} + \mathbf{D}' \mathbf{q}, \quad (\text{A.3d})$$

$$\mathbf{g} = \mathbf{C}' \mathbf{q} - \mathbf{D}' \mathbf{p}, \quad (\text{A.3e})$$

such that for the MInt,<sup>66,68</sup>

$$\mathbf{M}_{\text{M},H_{2,\text{MMST}}} = \begin{bmatrix} 1 & \mathbf{0}^T & 0 & \mathbf{0}^T \\ \mathbf{g} & \mathbf{C} & \mathbf{0} & -\mathbf{D} \\ b & \mathbf{e} & 1 & \mathbf{a} \\ \mathbf{f} & \mathbf{D} & \mathbf{0} & \mathbf{C} \end{bmatrix}, \quad (\text{A.4})$$

which is symplectic and satisfies Liouville's theorem,<sup>66,68</sup> such that the overall propagation of  $H_{1,\text{MMST}}$  and  $H_{2,\text{MMST}}$  is symplectic.<sup>66,67</sup>

## B. Equivalence to MInt

Here, we show the Spin-MInt is equivalent to the MInt by comparing the integration equations for  $H_2$ . We note that  $u_x$  can be expressed as,<sup>49</sup>

$$u_x = (\mathbf{q} - i\mathbf{p})^T \hat{S}_1 (\mathbf{q} + i\mathbf{p}), \quad (\text{B.1})$$

where  $\hat{S}_1 = \frac{1}{2} \begin{bmatrix} 0 & 1 \\ 1 & 0 \end{bmatrix}$  is the first Pauli spin matrix and from Eqn. (10),<sup>65,86,87</sup>

$$\dot{\mathbf{q}} + i\dot{\mathbf{p}} = -i\mathbf{V}(\mathbf{q} + i\mathbf{p}), \quad (\text{B.2})$$

such that,

$$\dot{u}_x = i(\mathbf{q} - i\mathbf{p})^T [\mathbf{V}, \hat{S}_1] (\mathbf{q} + i\mathbf{p}), \quad (\text{B.3})$$

where  $\mathbf{V}$  is real and symmetric. Decomposing  $\mathbf{V}$  into traceless and identity-like components where,

$$\mathbf{V} = \begin{bmatrix} \frac{V_1 - V_2}{2} & \Delta \\ \Delta & \frac{V_2 - V_1}{2} \end{bmatrix} + \frac{V_1 + V_2}{2} \mathbb{I}. \quad (\text{B.4})$$

The commutator is then,

$$[\mathbf{V}, \hat{S}_1] = i(V_1 - V_2) \hat{S}_2, \quad (\text{B.5})$$

where  $\hat{S}_2$  is the second Pauli matrix. Substituting into Eqn. (B.3) and repeating for  $u_y$  and  $u_z$  results in Eqn. (37) which we integrate exactly. Therefore, the MInt and Spin-MInt electronic evolutions are equivalent.

We now do the same for the nuclear momentum propagation, comparing the integrated forms of  $P$  as alternative integration methods have been shown to produce different results in previous work.<sup>66</sup> The Spin-MInt propagation of  $P$  in Eqn. (45) is equivalent to,

$$P_{\text{SM}}(t + \Delta t) = P(t) - \Delta t \left( \mathbf{V}'_0 + \frac{1}{2} \text{Tr}[\mathbf{V}'] \right) - \frac{1}{2} \text{Tr}[(\mathbf{E} + i\mathbf{F})\mathbf{C}(\mathbf{u}, 0)], \quad (\text{B.6})$$

as outlined in Section IC of the Supplementary Material where,

$$\mathbf{C}(\mathbf{u}) = \begin{bmatrix} u_z & u_x - iu_y \\ u_x + iu_y & -u_z \end{bmatrix}, \quad (\text{B.7})$$

which is related to the  $\mathbf{C}(\mathbf{q}, \mathbf{p}) = (\mathbf{q} + i\mathbf{p}) \otimes (\mathbf{q} - i\mathbf{p})^T$  matrix,<sup>65,86</sup>

$$\mathbf{C}(\mathbf{q}, \mathbf{p}) = \mathbf{C}(\mathbf{u}) + 2r_s \mathbb{I}, \quad (\text{B.8})$$

such that we obtain the MInt  $P$  propagation, Eqn. (19),

$$P_{\text{SM}}(t + \Delta t) = P(t) - \Delta t \left( V'_0(R) + \frac{1}{2} \text{Tr}[\mathbf{V}'(R)] \right) - \frac{1}{2} \text{Tr}[(\mathbf{E} + i\mathbf{F})(\mathbf{C}(\mathbf{q}, \mathbf{p}, t) - 2r_s \mathbb{I})] \quad (\text{B.9a})$$

$$= P(t) - \Delta t \left( V'_0(R) - \frac{\gamma}{2} \text{Tr}[\mathbf{V}'(R)] \right) - \frac{1}{2} \text{Tr}[(\mathbf{E} + i\mathbf{F})\mathbf{C}(\mathbf{q}, \mathbf{p}, t)], \quad (\text{B.9b})$$

due to the symmetry of  $\mathbf{E}/\mathbf{F}$  and  $\text{Tr}[\mathbf{E}] = \text{Tr}[\mathbf{V}']\Delta t$ .<sup>68</sup> Hence, both algorithms are equivalent. We have chosen to propagate Eqn. (45) in the Spin-MInt algorithm to reduce computational cost.

### C. Spin-MInt Monodromy Matrices

For  $H_{1,\text{SM}}$ , only  $R$  is propagated and so similar to the MInt,<sup>66</sup>

$$\mathbf{M}_{\text{SM},H_{1,\text{SM}}} = \begin{bmatrix} 1 & 0 & \Delta t/2m & 0 \\ 0 & 1 & 0 & 0 \\ 0 & 0 & 1 & 0 \\ 0 & 0 & 0 & 1 \end{bmatrix}, \quad (\text{C.1})$$

which is easily shown to be symplectic.<sup>66</sup>

For  $H_{2,\text{SM}}$ , this is significantly more complex. Defining the exponential matrix as,

$$\mathbf{Q} = e^{-i\mathbf{W}t} = \mathbf{S}_W e^{-i\mathbf{\Lambda}_W \Delta t} \mathbf{S}_W^\dagger, \quad (\text{C.2})$$

such that the  $n$ th row of  $e^{-i\mathbf{W}t}$  is the vector  $\mathbf{Q}_n$ . The propagation of  $\mathbf{u}$  is,

$$u_x(t) = \mathbf{Q}_1 \mathbf{u}(0), \quad (\text{C.3})$$

$$u_y(t) = \mathbf{Q}_2 \mathbf{u}(0), \quad (\text{C.4})$$

$$u_z(t) = \mathbf{Q}_3 \mathbf{u}(0). \quad (\text{C.5})$$

Repeating for the derivative of  $e^{-i\mathbf{W}t}$  with respect to  $R$ ,

$$\mathbf{Q}' = e^{-i\mathbf{W}t'} = \mathbf{S}_W' e^{-i\mathbf{\Lambda}_W \Delta t} \mathbf{S}_W^\dagger - i\Delta t \mathbf{S}_W e^{-i\mathbf{\Lambda}_W \Delta t} \mathbf{\Lambda}_W' \mathbf{S}_W^\dagger + \mathbf{S}_W e^{-i\mathbf{\Lambda}_W \Delta t} \mathbf{S}_W'^\dagger \quad (\text{C.6})$$

such that  $\mathbf{Q}'_n$  is the  $n$ -th row of  $\mathbf{Q}'$ . The eigenvalues, eigenvectors, and their derivatives are presented in Supplementary Material Section IB for the  $N = 2$  system where  $H_y = 0$ . For  $N > 2$ , there exists algorithms in the literature to compute these.<sup>68,88</sup> We define the derivatives of  $\mathbf{u}$  with respect to the conjugate variables as,

$$\mathbf{v}_1 = \frac{\partial \mathbf{u}}{\partial r_s \cos \theta} = \begin{bmatrix} -2 \cos \phi / \tan \theta \\ -2 \sin \phi / \tan \theta \\ 2 \end{bmatrix}, \quad (\text{C.7a})$$

$$\mathbf{v}_2 = \frac{\partial \mathbf{u}}{\partial \phi} = \begin{bmatrix} -u_y \\ u_x \\ 0 \end{bmatrix}. \quad (\text{C.7b})$$

We note that,

$$r_s \cos \theta(t) = \frac{1}{2} \mathbf{Q}_3 \mathbf{u}(0), \quad (\text{C.8})$$

and,

$$\tan \phi(t) = \frac{\mathbf{Q}_2 \mathbf{u}(0)}{\mathbf{Q}_1 \mathbf{u}(0)}, \quad (\text{C.9})$$

such that derivatives of  $\phi$  are,

$$\frac{\partial \phi(t)}{\partial f(0)} = \frac{u_x^2(t)}{u_x^2(t) + u_y^2(t)} \frac{\partial \tan \phi(t)}{\partial f(0)}, \quad (\text{C.10})$$

where  $f$  is a ghost variable and,

$$\frac{\partial \tan \phi(t)}{\partial \phi} = \sec^2 \phi(t) = \frac{u_x^2(t) + u_y^2(t)}{u_x^2(t)}, \quad (\text{C.11})$$

such that derivatives are obtained using the quotient rule.

We define the monodromy matrix as,

$$\mathbf{M}_{\text{SM}, H_2, \text{SM}} = \begin{bmatrix} 1 & 0 & 0 & 0 \\ a & b & 0 & c \\ d & e & 1 & f \\ g & h & 0 & j \end{bmatrix}, \quad (\text{C.12})$$

with,

$$a = \frac{u_x(\mathbf{Q}'_2 \mathbf{u}) - u_y(\mathbf{Q}'_1 \mathbf{u})}{u_x^2 + u_y^2}, \quad (\text{C.13a})$$

$$b = \frac{u_x(\mathbf{Q}_2 \mathbf{v}_2) - u_y(\mathbf{Q}_1 \mathbf{v}_2)}{u_x^2 + u_y^2}, \quad (\text{C.13b})$$

$$c = \frac{u_x(\mathbf{Q}_2 \mathbf{v}_1) - u_y(\mathbf{Q}_1 \mathbf{v}_1)}{u_x^2 + u_y^2}, \quad (\text{C.13c})$$

$$d = -\Delta t \left( \mathbf{v}_0'' + \frac{1}{2} \text{Tr}[\mathbf{v}'''] \right) - \frac{1}{2} \mathbf{H}'' \mathbf{S}_W \mathbf{r} \mathbf{S}_W^\dagger \mathbf{u} - \frac{1}{2} \mathbf{H}' (\mathbf{S}_W' \mathbf{r} \mathbf{S}_W^\dagger + \mathbf{S}_W \mathbf{r}' \mathbf{S}_W^\dagger + \mathbf{S}_W \mathbf{r} \mathbf{S}_W'^\dagger) \mathbf{u}, \quad (\text{C.13d})$$

$$e = -\frac{1}{2} \mathbf{H}' \mathbf{S}_W \mathbf{r} \mathbf{S}_W^\dagger \mathbf{v}_2, \quad (\text{C.13e})$$

$$f = -\frac{1}{2} \mathbf{H}' \mathbf{S}_W \mathbf{r} \mathbf{S}_W^\dagger \mathbf{v}_1, \quad (\text{C.13f})$$

$$g = \frac{1}{2} \mathbf{Q}'_3 \mathbf{u}, \quad (\text{C.13g})$$

$$h = \frac{1}{2} \mathbf{Q}_3 \mathbf{v}_2, \quad (\text{C.13h})$$

$$j = \frac{1}{2} \mathbf{Q}_3 \mathbf{v}_1, \quad (\text{C.13i})$$



where  $u_x/u_y/u_z$  are at evolved time,  $\mathbf{u}/\mathbf{v}_1/\mathbf{v}_2$  are at initial time and,

$$\Upsilon'_{nm} = \begin{cases} \frac{i\lambda'_n}{\lambda_n^2}(-i\Delta t \lambda_n e^{-i\lambda_n \Delta t} - (e^{-i\lambda_n \Delta t} - 1)) & n = m \quad \text{and} \quad \lambda_n \neq 0 \\ 0 & \text{otherwise,} \end{cases} \quad (\text{C.14})$$

is obtained from differentiation of Eqn. (44). The determinant is,

$$|\mathbf{M}_{\text{SM}, H_{2,\text{SM}}}| = jb - ch = 1, \quad (\text{C.15})$$

as shown in the Supplementary Material Section IE such that the Spin-MInt satisfies Liouville's theorem. The symplecticity criterion is,

$$\mathbf{M}_{\text{SM}, H_{2,\text{SM}}}^T \mathbf{J}^{-1} \mathbf{M}_{\text{SM}, H_{2,\text{SM}}} = \begin{bmatrix} 0 & C_1 & -1 & C_2 \\ -C_1 & 0 & 0 & -1 \\ 1 & 0 & 0 & 0 \\ -C_2 & 1 & 0 & 0 \end{bmatrix}, \quad (\text{C.16})$$

where we show that  $C_1 = -e - ah + gb = 0$  and  $C_2 = -f - ja + cg = 0$  in Section IF of the Supplementary Material, such that the Spin-MInt is rigorously symplectic.

## D. Angle-based Algorithm

An alternative algorithm for propagating spin-mapping variables is to propagate the angles directly.<sup>51,54</sup> The propagation for  $H_{1,\text{SM}}$  is identical to the MInt and Spin-MInt. For  $H_{2,\text{SM}}$ , a Velocity-Verlet step is performed in the spin-mapping angles followed by nuclear momentum propagation. The electronic EOM are,

$$r_s \cos \theta(\Delta t/2) = r_s \cos \theta(0) + 2\Delta r_s \sin \theta(0) \sin \phi(0) \Delta t/2, \quad (\text{D.1a})$$

$$\phi(\Delta t) = \phi(0) + \left( (V_1 - V_2) - 2\Delta \frac{\cos \phi(0)}{\tan \theta(\Delta t/2)} \right) \Delta t, \quad (\text{D.1b})$$

$$r_s \cos \theta(\Delta t) = r_s \cos \theta(\Delta t/2) + 2\Delta r_s \sin \theta(\Delta t/2) \sin \phi(\Delta t) \Delta t/2, \quad (\text{D.1c})$$

and the nuclear momentum propagation is,

$$P(t) = P(0) - (\mathbf{V}'_0 + (V'_1 - V'_2)r_s \cos \theta(\Delta t)). \quad (\text{D.2})$$

Alternatively,  $\theta$  can be propagated as propagating  $r_s \cos \theta$  is equivalent to utilising the chain rule.<sup>54</sup> The monodromy matrix is quite complex,

$$\mathbf{M}_{\theta-\phi, H_{2,\text{SM}}} = \mathbf{M}_P \mathbf{M}_{r_s \cos \theta(\Delta t)} \mathbf{M}_{\phi(\Delta t)} \mathbf{M}_{r_s \cos \theta(\Delta t/2)}, \quad (\text{D.3})$$

where we specify the elements that deviate from the identity matrix,

$$\mathbf{M}_{P,31} = -(\mathbf{V}_0'' + (V_1'' - V_2'')r_s \cos \theta(\Delta t))\Delta t, \quad (\text{D.4a})$$

$$\mathbf{M}_{P,34} = (V_1' - V_2')r_s \sin \theta(\Delta t)\Delta t, \quad (\text{D.4b})$$

$$\mathbf{M}_{r_s \cos \theta(\Delta t),42} = 2\Delta r_s \sin \theta(\Delta t/2) \cos \phi(\Delta t)\Delta t/2, \quad (\text{D.4c})$$

$$\mathbf{M}_{r_s \cos \theta(\Delta t),44} = 1 - 2\Delta \frac{\sin \phi(\Delta t)}{\tan \theta(\Delta t/2)}\Delta t/2, \quad (\text{D.4d})$$

$$\mathbf{M}_{\phi(\Delta t),21} = (V_1' - V_2')\Delta t, \quad (\text{D.4e})$$

$$\mathbf{M}_{\phi(\Delta t),22} = 1 + 2\Delta \frac{\sin \phi(0)}{\tan \theta(\Delta t/2)}\Delta t, \quad (\text{D.4f})$$

$$\mathbf{M}_{\phi(\Delta t),24} = -2\Delta \frac{\cos \phi(0)}{r_s \sin^3 \theta(\Delta t/2)}\Delta t, \quad (\text{D.4g})$$

$$\mathbf{M}_{r_s \cos \theta(\Delta t/2),42} = 2\Delta r_s \sin \theta(0) \cos \phi(0)\Delta t/2, \quad (\text{D.4h})$$

$$\mathbf{M}_{r_s \cos \theta(\Delta t/2),44} = 1 - 2\Delta \frac{\sin \phi(0)}{\tan \theta(0)}\Delta t/2, \quad (\text{D.4i})$$

and the determinant is,

$$|\mathbf{M}_{\theta-\phi, H_{2,SM}}| = \mathbf{M}_{r_s \cos \theta(\Delta t),44} \times \mathbf{M}_{\phi(\Delta t),22} \times \mathbf{M}_{r_s \cos \theta(\Delta t/2),44} \quad (\text{D.5})$$

$$= 1 + \mathcal{O}(\Delta t), \quad (\text{D.6})$$

such that Liouville's theorem is satisfied on the order of  $\Delta t$ . Evaluating the symplecticity criterion for each of these matrices results in terms that differ from the criterion on order of  $\Delta t$ . Hence, this algorithm is unlikely to be symplectic for a finite timestep.

## E. Generalisation to Multiple Nuclear and Electronic States

Here, we generalise the Spin-MInt algorithm to multiple nuclear and electronic states. The nuclear states,  $K$ , is straightforward and follows the same form as seen in Ref. [68]. The electronic states,  $N$ , is more complex and we need to shift the formalism from the 3 dimensional Lie group  $SU(2)$  to the  $N^2 - 1$  dimensional  $SU(N)$ .<sup>49,51</sup>

We first define a basis of the Lie algebra  $SU(N)$  which replaces the Pauli spin matrices. These are the Generalised Gell-Mann (GGM) matrices,<sup>51,89,90</sup> where we obtain  $N^2 - 1$  matrices,  $\hat{S}_i$  where  $i \in \{1, \dots, N^2 - 1\}$ . This comprises of  $N(N - 1)/2$  symmetric matrices,

$$\hat{S}_{\alpha_{nm}} = E_{mn} + E_{nm}, \quad (\text{E.1})$$

$N(N-1)/2$  antisymmetric matrices,

$$\hat{S}_{\beta_{nm}} = -i(E_{mn} - E_{nm}), \quad (\text{E.2})$$

and  $N-1$  diagonal matrices,

$$\hat{S}_{\gamma_n} = \sum_{l=1}^{n-1} \left( \sqrt{\frac{2}{n(n-1)}} E_{ll} \right) - \sqrt{\frac{2(n-1)}{n}} E_{nn}, \quad (\text{E.3})$$

where  $E_{nm}$  is a  $N \times N$  matrix with 1 in the  $(n, m)$ -th position and 0 elsewhere and,

$$\alpha_{nm} = n^2 + 2(m-n) - 1, \quad (\text{E.4})$$

$$\beta_{nm} = n^2 + 2(m-n), \quad (\text{E.5})$$

$$\gamma_n = n^2 - 1, \quad (\text{E.6})$$

for  $1 \leq m < n \leq N$  and  $2 \leq n \leq N$ .<sup>51</sup> These are ordered conventionally following the literature.<sup>91,92</sup>

The spin-vector for  $N$  states as spin-coherent states is,<sup>49,51</sup>

$$|\mathbf{\Omega}\rangle = \sum_{n=1}^N |n\rangle \langle n|\mathbf{\Omega}\rangle, \quad (\text{E.7})$$

where the expansion coefficients are,

$$\langle n|\mathbf{\Omega}\rangle_N = \begin{cases} \langle n|\mathbf{\Omega}\rangle_{N-1} & 1 \leq n < N-1 \\ \langle N-1|\mathbf{\Omega}\rangle_{N-1} \cos \frac{\theta_N}{2} & n = N-1 \\ \langle N-1|\mathbf{\Omega}\rangle_{N-1} e^{i\phi_N} \sin \frac{\theta_N}{2} & n = N, \end{cases} \quad (\text{E.8})$$

which are defined recursively from  $\langle 1|\mathbf{\Omega}\rangle_1 = 1$  such that,

$$\Omega_{\alpha_{nm}} = \langle \mathbf{\Omega} | \hat{S}_{\alpha_{nm}} | \mathbf{\Omega} \rangle, \quad (\text{E.9})$$

and likewise for the antisymmetric and diagonal GGM matrices.<sup>49</sup> The angles are the general Euler angles in a multidimensional Bloch sphere where  $N-1$  spheres are obtained such that  $\theta_n \in [0, \pi]$  and  $\phi_n \in [0, 2\pi]$  and further details can be found in the literature.<sup>49,51</sup>

Here, we express the  $N^2 - 1$  dimensional spin-vector in terms of the MMST variables where,

$$2r_s \Omega_{\alpha_{nm}} = (\mathbf{q} - i\mathbf{p})^T \hat{S}_{\alpha_{nm}} (\mathbf{q} + i\mathbf{p}) \quad (\text{E.10})$$

$$= \text{Tr}[\hat{S}_{\alpha_{nm}} \mathbf{C}(\mathbf{q}, \mathbf{p})], \quad (\text{E.11})$$

and likewise for the antisymmetric and diagonal GGM matrices where  $\mathbf{C} = (\mathbf{q} + i\mathbf{p}) \otimes (\mathbf{q} - i\mathbf{p})^T$ .<sup>51</sup> The squared radius of the hyper-sphere is,

$$R^2 = \sum_{n=1}^N (q_n^2 + p_n^2) \equiv 2r_s, \quad (\text{E.12})$$

where the radius is often set by the Stratonovich-Weyl kernel used and  $r_s$  here is twice what is used earlier for  $N = 2$ .<sup>44,49,51</sup> For example, with the  $W$  kernel used for the three-state model in Figure 7,  $r_s = \sqrt{N+1}$  such that  $R^2 = 2\sqrt{N+1}$ .<sup>49,51</sup> Other kernels can be seen in the literature.<sup>44,49</sup>

The generalised spin-mapping Hamiltonian is,

$$H_{\text{SM}}(\mathbf{\Omega}) = \frac{1}{2} \mathbf{P}^T \boldsymbol{\mu}^{-1} \mathbf{P} + \mathbf{V}_0(\mathbf{R}) + \frac{1}{N} \text{Tr}[\mathbf{V}(\mathbf{R})] + \frac{1}{2} \mathbf{H} \cdot (2r_s \mathbf{\Omega}), \quad (\text{E.13})$$

where  $\mathbf{R}$  and  $\mathbf{P}$  are  $K$  dimensional vectors of nuclear position and momentum,  $\boldsymbol{\mu}$  is a  $K \times K$  diagonal matrix of nuclear masses and the diabatic potential energy matrices are now  $N \times N$ .<sup>51,68</sup> This is equivalent to the MMST Hamiltonian where  $\gamma = 2(r_s - 1)/N$ .  $\mathbf{H}$  can be calculated by,

$$H_{\alpha_{nm}} = 2 \text{Tr}[\mathbf{V}(\mathbf{R}) \hat{S}_{\alpha_{nm}}], \quad (\text{E.14})$$

and likewise for the antisymmetric and diagonal matrices.<sup>51</sup> Splitting this Hamiltonian results in,

$$H_{1,\text{SM}} = \frac{1}{2} \mathbf{P}^T \boldsymbol{\mu}^{-1} \mathbf{P}, \quad (\text{E.15})$$

$$H_{2,\text{SM}} = \mathbf{V}_0(\mathbf{R}) + \frac{1}{N} \text{Tr}[\mathbf{V}(\mathbf{R})] + \frac{1}{2} \mathbf{H} \cdot (2r_s \mathbf{\Omega}), \quad (\text{E.16})$$

such that the propagation of  $H_{1,\text{SM}}$  for half a timestep is,

$$R_k(\Delta t/2) = R_k(0) + \frac{P_k(0)\Delta t}{4\mu_{kk}}, \quad (\text{E.17})$$

which is seen in Ref. [68]. For  $H_{2,\text{SM}}$ , the derivative equations of motion for  $\mathbf{\Omega}$  can be written in terms of structure constants detailed in Appendix A of Ref. [51],

$$\dot{\Omega}_i = \frac{-i}{2} \text{Tr}\{\hat{S}_i[V, S_k]\} \Omega_k = f_{ijk} H_j \Omega_k. \quad (\text{E.18})$$

The  $\mathbf{W}$  matrix is the adjoint representation of the potential matrix,  $\mathbf{V}(\mathbf{R})$ , in the  $\text{SU}(N)$  Lie group,<sup>92</sup> which can be calculated by,

$$W_{ab} = \frac{1}{2} \text{Tr}\{\hat{S}_a[\mathbf{V}, \hat{S}_b]\} = if_{ijk} H_j, \quad (\text{E.19})$$

which is easily shown to give the  $\mathbf{W}$  defined earlier for  $N = 2$ . The integration of Eqn. (E.18) follows Eqn. (40),

$$\mathbf{\Omega}(t + \Delta t) = \mathbf{S}_W e^{-i\mathbf{\Lambda}_W \Delta t} \mathbf{S}_W^\dagger \mathbf{\Omega}(t), \quad (\text{E.20})$$

and the propagation of  $\mathbf{P}$  is,

$$P_k(t + \Delta t) = P_k(t) - \Delta t \left( \mathbf{V}_0^k + \frac{1}{N} \text{Tr}[\mathbf{V}^k] \right) - \frac{1}{2} \mathbf{H}^k \mathbf{S}_W \mathbf{Y} \mathbf{S}_W^\dagger \mathbf{\Omega}(t), \quad (\text{E.21})$$

where  $\mathbf{V}^k$  is the derivative of  $\mathbf{V}$  with respect to  $R_k$  and likewise for any powers of  $k$ . All eigenvalues of  $\mathbf{W}$  used to calculate  $\mathbf{Y}$ , Eqn (44), are in  $\pm\lambda$  non-zero pairs for even  $N^2 - 1$ . For odd  $N^2 - 1$ , there is an additional zero eigenvalue. The eigenvalue and eigenvector derivatives are not required for trajectory propagation, only when calculating the monodromy, and for  $N > 2$  algorithms exist in the literature.<sup>88</sup>

We recover the previous propagation equations when  $K = 1$  and  $N = 2$ , leading us to believe that the generalised Spin-MInt algorithm is accurate and symplectic for all  $N > 2$ .

## REFERENCES

- <sup>1</sup>M. H. Beck, A. Jäckle, G. A. Worth, and H. D. Meyer, Phys. Rep. **324**, 1 (2000).
- <sup>2</sup>A. Van Haeften, C. Ash, and G. Worth, J. Chem. Phys. **159**, 194114 (2023).
- <sup>3</sup>H. Wang and M. Thoss, J. Chem. Phys. **119**, 1289 (2003).
- <sup>4</sup>S. Shin and H. Metiu, J. Phys. Chem. **100**, 7867 (1996).
- <sup>5</sup>S. Mukherjee, Y. Lassmann, R. S. Mattos, B. Demoulin, B. F. E. Curchod, and M. Barbatti, J. Chem. Theory Comput. **21**, 29 (2025).
- <sup>6</sup>T. J. H. Hele, M. J. Willatt, A. Muolo, and S. C. Althorpe, J. Chem. Phys. **142**, 134103 (2015).
- <sup>7</sup>J. Cao and G. A. Voth, J. Chem. Phys. **99**, 10070 (1993).
- <sup>8</sup>J. Cao and G. A. Voth, J. Chem. Phys. **100**, 5106 (1994).
- <sup>9</sup>J. Cao and G. A. Voth, J. Chem. Phys. **101**, 6157 (1994).
- <sup>10</sup>J. Cao and G. A. Voth, J. Chem. Phys. **100**, 5093 (1994).
- <sup>11</sup>M. Rossi, M. Ceriotti, and D. E. Manolopoulos, J. Chem. Phys. **140**, 234116 (2014).
- <sup>12</sup>G. Stock and M. Thoss, Phys. Rev. Lett. **78**, 578 (1997).
- <sup>13</sup>W. H. Miller, J. Chem. Phys. **53**, 3578 (1970).
- <sup>14</sup>T. J. H. Hele, M. J. Willatt, A. Muolo, and S. C. Althorpe, J. Chem. Phys. **142**, 191101 (2015).

- <sup>15</sup>T. J. H. Hele and Y. V. Suleimanov, J. Chem. Phys. **143**, 074107 (2015), arXiv:1506.07460.
- <sup>16</sup>T. J. H. Hele, Mol. Phys. **114**, 1461 (2016).
- <sup>17</sup>S. Jang and G. A. Voth, J. Chem. Phys. **111**, 2371 (1999).
- <sup>18</sup>S. Jang and G. A. Voth, J. Chem. Phys. **111**, 2357 (1999).
- <sup>19</sup>I. R. Craig and D. E. Manolopoulos, J. Chem. Phys. **121**, 3368 (2004).
- <sup>20</sup>M. Ceriotti, M. Parrinello, T. E. Markland, and D. E. Manolopoulos, J. Chem. Phys. **133**, 124104 (2010).
- <sup>21</sup>S. Habershon, D. E. Manolopoulos, T. E. Markland, and T. F. Miller III, Annu. Rev. Phys. Chem. **64**, 387 (2013).
- <sup>22</sup>X. Sun, H. Wang, and W. H. Miller, J. Chem. Phys. **109**, 4190 (1998).
- <sup>23</sup>X. Sun, H. Wang, and W. H. Miller, J. Chem. Phys. **109**, 7064 (1998).
- <sup>24</sup>Q. Shi and E. Geva, J. Phys. Chem. A **108**, 6109 (2004).
- <sup>25</sup>H. Wang, X. Sun, and W. H. Miller, J. Chem. Phys. **108**, 9726 (1998).
- <sup>26</sup>H. Wang, X. Song, D. Chandler, and W. H. Miller, J. Chem. Phys. **110**, 4828 (1999).
- <sup>27</sup>T. J. H. Hele, *An Electronically Non-Adiabatic Generalization of Ring Polymer Molecular Dynamics*, Ph.D. thesis, University of Oxford (2011).
- <sup>28</sup>J. O. Richardson and M. Thoss, J. Chem. Phys. **139**, 031102 (2013).
- <sup>29</sup>N. Ananth, J. Chem. Phys. **139**, 124102 (2013).
- <sup>30</sup>N. Ananth, C. Venkataraman, and W. H. Miller, J. Chem. Phys. **127**, 084114 (2007).
- <sup>31</sup>M. S. Church, S. V. Antipov, and N. Ananth, J. Chem. Phys. **146**, 234104 (2017).
- <sup>32</sup>S. V. Antipov, Z. Ye, and N. Ananth, J. Chem. Phys. **142**, 184102 (2015).
- <sup>33</sup>J. Liu, Int. J. Quantum Chem. **115**, 657 (2015).
- <sup>34</sup>V. Filinov, Nucl. Phys. B **271**, 717 (1986).
- <sup>35</sup>M. Thoss, H. Wang, and W. H. Miller, J. Chem. Phys. **114**, 9220 (2001).
- <sup>36</sup>R. Kapral, Chem. Phys. **481**, 77 (2016).
- <sup>37</sup>J. C. Tully and R. K. Preston, J. Chem. Phys. **55**, 562 (1971).
- <sup>38</sup>J. C. Tully, J. Chem. Phys. **137**, 22A301 (2012).
- <sup>39</sup>F. A. Shakib and P. Huo, J. Phys. Chem. Lett. **8**, 3073 (2017).
- <sup>40</sup>D. V. Shalashilin, Faraday Discuss. **153**, 105 (2011).
- <sup>41</sup>T. Zimmermann and J. Vaníček, J. Chem. Phys. **141**, 134102 (2014).
- <sup>42</sup>H.-D. Meyer and W. H. Miller, J. Chem. Phys. **70**, 3214 (1979).
- <sup>43</sup>G. Stock and M. Thoss, in *Advances in Chemical Physics*, Vol. 131, edited by S. A. Rice (John

- Wiley & Sons, 2005) pp. 243–375.
- <sup>44</sup>J. E. Runeson and J. O. Richardson, *J. Chem. Phys.* **151**, 044119 (2019).
  - <sup>45</sup>J. R. Mannouch and J. O. Richardson, *J. Chem. Phys.* **158**, 104111 (2023).
  - <sup>46</sup>S. C. Althorpe, N. Ananth, G. Angulo, R. D. Astumian, V. Beniwal, J. Blumberger, P. G. Bolhuis, B. Ensing, D. R. Glowacki, S. Habershon, S. Hammes-Schiffer, T. J. H. Hele, N. Makri, D. E. Manolopoulos, L. K. McKemmish, T. F. M. Iii, W. H. Miller, A. J. Mulholland, T. Nekipelova, E. Pollak, J. O. Richardson, M. Richter, P. R. Chowdhury, D. Shalashilin, and R. Szabla, *Faraday Discuss.* **195**, 311 (2017).
  - <sup>47</sup>S. Althorpe, G. Angulo, R. D. Astumian, V. Beniwal, P. G. Bolhuis, J. Brandão, J. Ellis, W. Fang, D. R. Glowacki, S. Hammes-Schiffer, T. J. H. Hele, H. Jónsson, T. Lelièvre, N. Makri, D. Manolopoulos, A. M. Mebel, G. Menzl, T. F. Miller, M. Parrinello, P. M. Piaggi, E. Pollak, P. Roy Chowdhury, E. Sanz, D. Shalashilin, E. Skúlason, R. Spezia, and S. Taraphder, *Faraday Discuss.* **195**, 671 (2016).
  - <sup>48</sup>T. R. Nelson, A. J. White, J. A. Bjorgaard, A. E. Sifain, Y. Zhang, B. Nebgen, S. Fernandez-Alberti, D. Mozyrsky, A. E. Roitberg, and S. Tretiak, *Chem. Rev.* **120**, 2215 (2020).
  - <sup>49</sup>J. E. Runeson and J. O. Richardson, *J. Chem. Phys.* **152**, 084110 (2020).
  - <sup>50</sup>J. E. Runeson and J. O. Richardson, *Phys. Rev. Lett.* **127**, 250403 (2021).
  - <sup>51</sup>D. Bossion, W. Ying, S. N. Chowdhury, and P. Huo, *J. Chem. Phys.* **157**, 084105 (2022).
  - <sup>52</sup>U. Müller and G. Stock, *J. Chem. Phys.* **111**, 77 (1999).
  - <sup>53</sup>G. Stock and U. Müller, *J. Chem. Phys.* **111**, 65 (1999).
  - <sup>54</sup>D. Bossion, S. N. Chowdhury, and P. Huo, *J. Chem. Phys.* **154**, 184106 (2021).
  - <sup>55</sup>D. Bossion, S. N. Chowdhury, and P. Huo, *J. Chem. Phys.* **158**, 044123 (2023).
  - <sup>56</sup>J. R. Mannouch and J. O. Richardson, *J. Chem. Phys.* **153**, 194109 (2020).
  - <sup>57</sup>J. R. Mannouch and J. O. Richardson, *J. Chem. Phys.* **153**, 194110 (2020).
  - <sup>58</sup>J. R. Mannouch and J. O. Richardson, *J. Chem. Phys.* **156**, 024108 (2022).
  - <sup>59</sup>G. Amati, J. E. Runeson, and J. O. Richardson, *J. Chem. Phys.* **158**, 064113 (2023).
  - <sup>60</sup>J. E. Lawrence, J. R. Mannouch, and J. O. Richardson, *J. Chem. Phys.* **160**, 244112 (2024).
  - <sup>61</sup>J. A. Geuther, K. Asnaashari, and J. O. Richardson, *J. Chem. Theory Comput.* **21**, 2179 (2025).
  - <sup>62</sup>J. O. Richardson, J. E. Lawrence, and J. R. Mannouch, *Annu. Rev. Phys. Chem.* **76**, 663 (2025).
  - <sup>63</sup>J. E. Runeson, T. P. Fay, and D. E. Manolopoulos, *Phys. Chem. Chem. Phys.* **26**, 4929 (2024).
  - <sup>64</sup>D. Furlanetto and J. O. Richardson, *J. Phys. Chem. Lett.* **16**, 6794 (2025).
  - <sup>65</sup>L. E. Cook and T. J. H. Hele, *J. Chem. Phys.* **163**, 174113 (2025).

- <sup>66</sup>L. E. Cook, J. E. Runeson, J. O. Richardson, and T. J. H. Hele, *J. Chem. Theory Comput.* **19**, 6109 (2023).
- <sup>67</sup>B. Leimkuhler and S. Reich, *Simulating Hamiltonian Dynamics* (Cambridge University Press, 2005).
- <sup>68</sup>M. S. Church, T. J. H. Hele, G. S. Ezra, and N. Ananth, *J. Chem. Phys.* **148**, 102326 (2018).
- <sup>69</sup>S. Bonella and D. F. Coker, *J. Chem. Phys.* **114**, 7778 (2001).
- <sup>70</sup>A. Kelly, R. van Zon, J. Schofield, and R. Kapral, *J. Chem. Phys.* **136**, 084101 (2012).
- <sup>71</sup>J. O. Richardson, P. Meyer, M.-O. Pleinert, and M. Thoss, *Chem. Phys.* **482**, 124 (2017).
- <sup>72</sup>J. Tranchida, S. J. Plimpton, P. Thibaudeau, and A. P. Thompson, *J. Comput. Phys.* **372**, 406 (2018).
- <sup>73</sup>R. Prasad, S. Panda, and B. Hazra, *Probabilistic Engineering Mechanics* **74**, 103526 (2023).
- <sup>74</sup>A. Ivanov, S. Andrianov, N. Kulabukhova, R. Maier, Y. Senichev, and D. Zyuzin, in *IPAC 2013 Proc. 4th Int. Part. Accel. Conf.* (2013) pp. 2582–2584.
- <sup>75</sup>C. Lubich, B. Walther, and B. Brueggemann, *Phys. Rev. D* **81**, 104025 (2010).
- <sup>76</sup>R. I. McLachlan, K. Modin, and O. Verdier, *Phys. Rev. E* **89**, 061301 (2014).
- <sup>77</sup>J. Frank, W. Huang, and B. Leimkuhler, *J. Comput. Phys.* **133**, 160 (1997).
- <sup>78</sup>Z. Huang, H. Wang, and B. Xu, “Symplectic Spin-Lattice Dynamics with Machine-Learning Potentials,” (2025), arXiv:2506.12877 [cond-mat].
- <sup>79</sup>M. Irigoyen, in *Encyclopedia of Mathematical Physics* (Elsevier, 2006) pp. 624–630.
- <sup>80</sup>E. Hairer, C. Lubich, and G. Wanner, *Geometric Numerical Integration. Structure-Preserving Algorithms for Ordinary Differential Equations*, 2nd ed., Vol. 31 (Springer, 2006).
- <sup>81</sup>E. Luesink, S. Ephrati, P. Cifani, and B. Geurts, *Adv. Contin. Discrete Models* **2024**, 1 (2024).
- <sup>82</sup>D. J. Hardy and D. I. Okunbor, *J. Chem. Phys.* **102**, 8978 (1995).
- <sup>83</sup>M. E. Tuckerman, *Statistical Mechanics: Theory and Molecular Simulation* (Oxford University Press, 2010).
- <sup>84</sup>G. S. Ezra, *J. Math. Chem.* **35**, 29 (2004).
- <sup>85</sup>E. A. Coronado, J. Xing, and W. H. Miller, *Chem. Phys. Lett.* **349**, 521 (2001).
- <sup>86</sup>T. J. Hele and N. Ananth, *Faraday Discuss.* **195**, 269 (2016).
- <sup>87</sup>S. N. Chowdhury and P. Huo, *J. Chem. Phys.* **154**, 124124 (2021).
- <sup>88</sup>J. R. Magnus, *Econom. Theory* **1**, 179 (1985).
- <sup>89</sup>M. Gell-Mann, *Phys. Rev.* **125**, 1067 (1962).
- <sup>90</sup>T. Tilma and K. Nemoto, *J. Phys. A: Math. Theor.* **45**, 015302 (2011).



<sup>91</sup>R. A. Bertlmann and P. Krammer, J. Phys. A: Math. Theor. **41**, 235303 (2008).

<sup>92</sup>W. Pfeifer, *The Lie Algebras  $Su(N)$*  (Springer, 2003).